Conformational dynamics of Rouse chains during creep/recovery processes: a review

2005 J. Phys.: Condens. Matter 17 R607

(http://iopscience.iop.org/0953-8984/17/19/R01)

INSTITUTE OF PHYSICS PUBLISHING JOURNAL OF PHYSICS: CONDENSED MATTER

J. Phys.: Condens. Matter **17** (2005) R607–R636 doi:10.1088/0953-8984/17/19/R01

TOPICAL REVIEW

Conformational dynamics of Rouse chains during creep/recovery processes: a review

Hiroshi Watanabe and Tadashi Inoue

Institute for Chemical Research, Kyoto University, Uji, Kyoto 611-0011, Japan

E-mail: hiroshi@scl.kyoto-u.ac.jp

Received 7 December 2004, in final form 7 March 2005
Published 29 April 2005
Online at stacks.iop.org/JPhysCM/17/R607

Abstract

The Rouse model is a well-established model for non-entangled polymer chains and also serves as a fundamental model for entangled chains. The dynamic behaviour of this model under strain-controlled conditions has been fully analysed in the literature. However, despite the importance of the Rouse model, no analysis has been made so far of the orientational anisotropy of the Rouse eigenmodes during the stress-controlled, creep and recovery processes.

For completeness of the analysis of the model, the Rouse equation of motion is solved to calculate this anisotropy for monodisperse chains and their binary blends during the creep/recovery processes. The calculation is simple and straightforward, but the result is intriguing in the sense that each Rouse eigenmode during these processes has a distribution in the retardation times. This behaviour, reflecting the interplay/correlation among the Rouse eigenmodes of different orders (and for different chains in the blends) under the *constant stress* condition, is quite different from the behaviour under rate-controlled flow (where each eigenmode exhibits retardation/relaxation associated with a single characteristic time). Furthermore, the calculation indicates that the Rouse chains exhibit affine deformation on sudden imposition/removal of the stress and the magnitude of this deformation is inversely proportional to the number of bond vectors per chain. In relation to these results, a difference between the creep and relaxation properties is also discussed for chains obeying multiple relaxation mechanisms (Rouse and reptation mechanisms).

(Some figures in this article are in colour only in the electronic version)

Contents

1. Introduction 608
2. Theoretical framework 609
   2.1. Rouse equation of motion 609
   2.2. Orientational anisotropy and stress 610

3. Results and discussion 611
3.1. Monodisperse Rouse chain with $N \gg 1$ 611
3.2. Binary blends of Rouse chains with $N \gg 1$ 618
3.3. Monodisperse Rouse chains with small N 621
3.4. Difference between retardation and relaxation properties 628
4. Concluding remarks 633
Appendix A. Solution of equation (24) 633
Appendix B. Solution of equation (32) 634
Appendix C. Affine deformation and effective strain for the bond vector 634
References 636

1. Introduction

The Rouse model, the simplest bead–spring model, is well established for flexible polymer chains [1–6]. This model has been frequently applied to non-entangled chains in concentrated systems. The model also serves as a fundamental ingredient in the description of the entanglement dynamics: the tube model for entangled chains analyses the motion of the Rouse chain confined in a tube-like regime for calculating various kinds of dynamic properties [4–6]. Thus, the Rouse model is one of the most important models in the field of polymer dynamics.

In this model, the mechanical stress reflects the orientational anisotropy of the chain segments that is often expressed in terms of the Rouse eigenmodes. The relaxation modulus $G(t)$ under a step shear strain is easily calculated from these eigenmodes, and all linear viscoelastic properties are straightforwardly calculated from this $G(t)$ within the phenomenological framework of linear viscoelasticity: for example, the complex viscosity η^* is given by the Fourier transformation of $G(t)$, and the creep compliance $J(t)$ is calculated through a convolution relationship [2, 4, 7],

$$\int_0^t \mathrm{d}t'\, G(t-t')J(t) = t. \tag{1}$$

Indeed, for the Rouse chain composed of a finite number (N) of beads, Berry [7] utilized equation (1) to numerically calculate $J(t)$ from $G(t)$. Furthermore, Lodge and Wu [8] formulated the constitutive equation for the Rouse chain: this equation gives the stress tensor as a function of the Finger strain tensor, thereby enabling us to calculate all kinds of nonlinear viscoelastic properties (such as the normal stress). Lodge [9] also constructed a rather general framework for calculating the shape/strain recovery of a material under various conditions with the aid of the constitutive equation.

In the above sense, the viscoelastic properties of the Rouse chains are well known. However, surprisingly, the time evolution of the orientational anisotropy of the Rouse eigenmodes during the *constant stress* creep/recovery processes was not examined previously in the long history of the study of polymer dynamics. Because of the importance of the Rouse model, the analysis of the conformational dynamics of the Rouse chain during the creep/recovery processes is strongly desired.

From this point of view, we recently solved the Rouse equation of motion to calculate the orientational anisotropy in the monodisperse systems [10] and binary blends [11] of the Rouse chains in the continuous limit. The calculation, based on the simple Laplace inversion method [12], was straightforward but the result was intriguing in the sense that each Rouse eigenmode has a distribution in the retardation time and does not exhibit the single Voigt-type retardation. This behaviour, reflecting interplay/correlation among the Rouse eigenmodes of *different orders* (and for different chains in the blends) under the constant stress condition, is

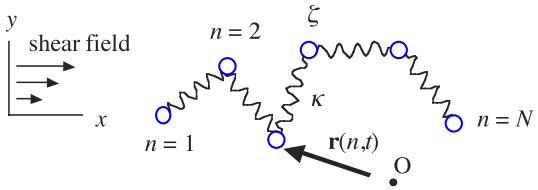

Figure 1. Schematic illustration of the Rouse chain.

quite different from the behaviour under rate-controlled flow where each eigenmode exhibits retardation/relaxation associated with a single characteristic time. Furthermore, the calculation for the Rouse chains with a finite bead number (N) showed that the chain deforms *affinely* on sudden imposition/removal of the stress and the magnitude of this deformation is inversely proportional to $N - 1$ [13].

This article presents a review of these results. The theoretical framework of the Rouse dynamics is briefly explained in section 2. In section 3, the orientational anisotropy during the creep/recovery processes is analysed for the monodisperse systems and blends of the Rouse chains with $N \gg 1$. Then, changes of the chain conformation on sudden imposition/removal of the stress are analysed for monodisperse Rouse chains with small and large N. In relation to these results, a difference between the creep and relaxation properties is discussed for chains obeying multiple relaxation mechanisms (Rouse and reptation mechanisms) [14]. Finally, section 4 gives a summary of this article.

2. Theoretical framework [4–6]

2.1. Rouse equation of motion

We consider a monodisperse system containing ν linear Rouse chains per unit volume. As shown in figure 1, each chain is composed of N segments (beads), and the neighbouring segments in the chain are connected by a Gaussian spring of the spring constant $\kappa = 3k_{\mathrm{B}}T/a^2$. Here, a is the average size of the segment (= root mean square length of the spring), k_{B} is the Boltzmann constant, and T is the absolute temperature. In the mean-field description of the chain motion, we focus on a given chain and regard the surrounding chains as a uniform frictional medium for the focused chain. The segmental friction coefficient of the focused chain in this medium is denoted by ζ.

A shear force or shear deformation is applied to the system. The x and y directions, respectively, are chosen to be the shear and shear gradient directions, as shown in figure 1. The flow velocity $\mathbf{V}(n, t)$ of the frictional medium at the position $\mathbf{r}(n, t)$ of the nth segment of the focused chain at time t is determined by the applied force/deformation. A uniform shear field characterized with a position-independent shear rate $\dot{\gamma}(t)$ is generated by the small force/deformation in the linear viscoelastic regime. Then, $\mathbf{V}(n, t)$ is expressed in terms of this $\dot{\gamma}(t)$ and the y component of the position vector of the nth segment, $r_y(n, t)$, as

$$\mathbf{V}(n,t) = \begin{bmatrix} \dot{\gamma}(t) r_y(n,t) \\ 0 \\ 0 \end{bmatrix}. \tag{2}$$

Changes of $\mathbf{r}(n, t)$ with t are fully described by the discrete version of the Rouse equation of

motion incorporating this $\mathbf{V}$,

$$\varsigma\frac{\partial}{\partial t}\begin{bmatrix}\mathbf{r}(1,t)\\ \mathbf{r}(2,t)\\ \cdots\\ \cdots\\ \mathbf{r}(N,t)\end{bmatrix}-\varsigma\begin{bmatrix}\mathbf{V}(1,t)\\ \mathbf{V}(2,t)\\ \cdots\\ \cdots\\ \mathbf{V}(N,t)\end{bmatrix}=\kappa\mathbf{A}\cdot\begin{bmatrix}\mathbf{r}(1,t)\\ \mathbf{r}(2,t)\\ \cdots\\ \cdots\\ \mathbf{r}(N,t)\end{bmatrix}+\begin{bmatrix}\mathbf{F}(1,t)\\ \mathbf{F}(2,t)\\ \cdots\\ \cdots\\ \mathbf{F}(N,t)\end{bmatrix}. \tag{3}$$

Here, $\mathbf{F}(n,t)$ represents the Brownian force acting on the nth segment at time t, and $\mathbf{A}$ is the well-known Rouse matrix given by

$$\mathbf{A}=\begin{bmatrix}-1 & 1 & 0 & 0 & \cdots & 0\\ 1 & -2 & 1 & 0 & \cdots & 0\\ 0 & 1 & -2 & 1 & \cdots & 0\\ \cdots & \cdots & \cdots & \cdots & \cdots & \cdots\\ 0 & \cdots & \cdots & 1 & -2 & 1\\ 0 & 0 & \cdots & \cdots & 1 & -1\end{bmatrix}. \tag{4}$$

$\mathbf{F}(n,t)$ is modelled as a white noise and characterized with the first- and second-order moments of its component F_α in the α-direction,

$$\langle F_\alpha(n,t)\rangle=0,\qquad \langle F_\alpha(n,t)F_\beta(m,t')\rangle=2\zeta k_{\mathrm{B}}T\delta_{nm}\delta(t-t')\delta_{\alpha\beta} \tag{5}$$

where $\langle\cdots\rangle$ denotes the average over the chains in the system.

For $N\to\infty$, $\mathbf{r}(n,t)$ is often treated as a continuous function of n and the range of n is simplified to be $0<n<N$ (instead of $1\leqslant n\leqslant N$). In this treatment, equation (3) is rewritten as the continuous version of the Rouse equation of motion:

$$\varsigma\left\{\frac{\partial\mathbf{r}(n,t)}{\partial t}-\mathbf{V}(n,t)\right\}=\kappa\frac{\partial^2\mathbf{r}(n,t)}{\partial n^2}+\mathbf{F}(n,t)\qquad\text{for } 0<n<N. \tag{6}$$

Here, $\mathbf{F}(n,t)$ represents the continuous version of the Brownian force characterized by

$$\langle F_\alpha(n,t)\rangle=0,\qquad \langle F_\alpha(n,t)F_\beta(m,t')\rangle=2\zeta k_{\mathrm{B}}T\delta(n-m)\delta(t-t')\delta_{\alpha\beta}. \tag{7}$$

The boundary condition for equation (6), representing the lack of external tensile forces acting at the chain ends, is given by

$$\frac{\partial\mathbf{r}(n,t)}{\partial n}=\mathbf{0}\qquad\text{for } n=0 \text{ and } N. \tag{8}$$

In the binary blends of Rouse chains, the above equation of motion (in either the discrete or the continuous version) is valid for each component chain. Thus, equations (2)–(8) fully specify the motion of the Rouse chains considered in this article.

2.2. Orientational anisotropy and stress

In the linear viscoelastic regime under small shear force/deformation, the orientational anisotropy of monodisperse Rouse chains is fully characterized with the orientation function defined by

$$S(n,t)=\frac{1}{a^2}\langle u_x(n,t)u_y(n,t)\rangle. \tag{9}$$

Here, $u_\alpha(n,t)$ is the α component of the bond vector $\mathbf{u}(n,t)$ ($\alpha=x,y$), with $\mathbf{u}(n,t)$ being defined by

$$\mathbf{u}(n,t)=\mathbf{r}(n+1,t)-\mathbf{r}(n,t)\qquad\text{(in discrete treatment)} \tag{10a}$$

$$\mathbf{u}(n,t)=\frac{\partial\mathbf{r}(n,t)}{\partial n}\qquad\text{(in continuous treatment).} \tag{10b}$$

The shear stress at time t, $\sigma(t)$, is simply related to a total orientational anisotropy as

$$\sigma(t) = 3\nu k_{\mathrm{B}}T \sum_{n=1}^{N-1} S(n,t) \qquad \text{(in discrete treatment)} \tag{11a}$$

$$\sigma(t) = 3\nu k_{\mathrm{B}}T \int_0^N \mathrm{d}n\, S(n,t) \qquad \text{(in continuous treatment).} \tag{11b}$$

For the blends of Rouse chains, the orientational anisotropy and stress for each component chain are specified by equations (9) and (11), respectively, and the total stress is given by a sum of the component stresses.

Thus, we can analyse the conformational changes of the Rouse chain during the creep/recovery processes by solving the equation of motion (equation (3) or (6)) to calculate $\mathbf{u}(n,t)$ and $S(n,t)$. Since the stress is kept constant during these processes, the shear rate $\dot{\gamma}(t)$ included in the equation of motion (through the $\mathbf{V}(n,t)$ term; see equations (2), (3), and (6)) is determined by the Rouse chain itself in such a way that the calculated $S(n,t)$ satisfies the constant stress condition. In other words, the equation of motion and the stress expression (equation (11)) should be coupled with each other for consistently calculating $\dot{\gamma}(t)$ and $S(n,t)$. This calculation, achieved by introducing Rouse eigenmodes, reveals interplay (correlation) of these eigenmodes due to this coupling, as demonstrated in the remaining part of this article.

3. Results and discussion

3.1. Monodisperse Rouse chain with $N \gg 1$ [10]

3.1.1. Eigenmode expansion and orientation function. For monodisperse Rouse chains having the bead number $N \gg 1$, we utilize the continuous version of the equation of motion (equation (6)) to calculate the orientation function $S(n,t)$ during the creep/recovery processes. Because of the boundary condition, equation (8), the segment position $\mathbf{r}(n,t)$ is conveniently expanded in the Rouse eigenmodes associated with the eigenfunctions $\cos(p\pi n/N)$,

$$\mathbf{r}(n,t) = \sum_{p=0}^{\infty} \begin{bmatrix} X_p(t) \\ Y_p(t) \\ Z_p(t) \end{bmatrix} \cos\left(\frac{p\pi n}{N}\right). \tag{12}$$

Here, $X_p(t)$, $Y_p(t)$, and $Z_p(t)$ are the amplitudes of the pth eigenmode in the x-, y-, and z-directions (shear, shear gradient, and vorticity directions), respectively.

From equations (2) and (12), the flow velocity $\mathbf{V}(n,t)$ is also expanded with respect to the Rouse eigenfunctions as

$$\mathbf{V}(n,t) = \sum_{p=0}^{\infty} \begin{bmatrix} \dot{\gamma}(t) Y_p(t) \\ 0 \\ 0 \end{bmatrix} \cos\left(\frac{p\pi n}{N}\right). \tag{13}$$

Equations (6), (12), and (13) give a set of time evolution equations for the eigenmode amplitudes $X_p(t)$ and $Y_p(t)$ (that determine the orientation function, as explained later). The results are summarized as [10]

$$\frac{\mathrm{d}X_p(t)}{\mathrm{d}t} = -\frac{\kappa p^2\pi^2}{\varsigma N^2} X_p(t) + \dot{\gamma}(t) Y_p(t) + \frac{1}{\varsigma} f_{x,p}(t) \tag{14}$$

$$\frac{\mathrm{d}Y_p(t)}{\mathrm{d}t} = -\frac{\kappa p^2\pi^2}{\varsigma N^2} Y_p(t) + \frac{1}{\varsigma} f_{y,p}(t). \tag{15}$$

Here, $f_{\alpha,p}(t)$ ($\alpha = x, y$; $p \geqslant 1$) is the Fourier component of the Brownian force $\mathbf{F}(n,t)$ defined by

$$f_{\alpha,p}(t) = \frac{2}{N}\int_0^N \mathrm{d}n\, F_\alpha(n,t)\cos\left(\frac{p\pi n}{N}\right) \qquad (\alpha = x, y). \tag{16}$$

This $f_{\alpha,p}(t)$ has the first- and second-moment averages (see equation (7))

$$\langle f_{\alpha,p}(t)\rangle = 0, \qquad \langle f_{\alpha,p}(t) f_{\beta,q}(t')\rangle = \frac{4\varsigma k_\mathrm{B}T}{N}\delta(t-t')\delta_{pq}\delta_{\alpha\beta}. \tag{17}$$

Equations (14) and (15) can be solved with a standard method to give

$$\begin{aligned} X_p(t) = {} & X_p(0)\exp\left(-\frac{p^2 t}{2\tau_\mathrm{R}}\right) + Y_p(0)\exp\left(-\frac{p^2 t}{2\tau_\mathrm{R}}\right)\int_0^t \mathrm{d}t'\,\dot\gamma(t') \\ & + \frac{1}{\varsigma}\int_0^t \mathrm{d}t'\,\exp\left(-\frac{p^2(t-t')}{2\tau_\mathrm{R}}\right) \\ & \times\left\{ f_{x,p}(t') + \dot\gamma(t')\int_0^{t'}\mathrm{d}t''\,\exp\left(-\frac{p^2(t'-t'')}{2\tau_\mathrm{R}}\right) f_{y,p}(t'')\right\} \end{aligned} \tag{18}$$

$$Y_p(t) = Y_p(0)\exp\left(-\frac{p^2 t}{2\tau_\mathrm{R}}\right) + \frac{1}{\varsigma}\int_0^t \mathrm{d}t'\,\exp\left(-\frac{p^2(t-t')}{2\tau_\mathrm{R}}\right) f_{y,p}(t'). \tag{19}$$

Here, τ_R is the longest viscoelastic relaxation time of the Rouse chain,

$$\tau_\mathrm{R} = \frac{\varsigma N^2}{2\pi^2\kappa} = \frac{\varsigma N^2 a^2}{6\pi^2 k_\mathrm{B}T}. \tag{20}$$

From equations (9), (10*b*), (12), (18), and (19), the orientation function is obtained as

$$S(n,t) = \frac{2\sigma_\mathrm{steady}}{\nu N k_\mathrm{B}T}\sum_{p=1}^{\infty} A_p(t)\sin^2\left(\frac{p\pi n}{N}\right) \tag{21}$$

where σ_steady is the stress in the steady state (=applied stress in the creep/recovery processes) and $A_p(t)$ is the normalized orientational anisotropy of the pth Rouse eigenmode defined by

$$A_p(t) = \frac{\nu k_\mathrm{B}T p^2\pi^2}{2\sigma_\mathrm{steady}a^2 N}\langle X_p(t)Y_p(t)\rangle. \tag{22}$$

During the creep/recovery processes of the Rouse chain, the cross-averages $\langle X_p(t)Y_q(t)\rangle$ with $p \neq q$ vanish, as shown later in equation (23). Thus, $S(n,t)$ is contributed only from $\langle X_p(t)Y_p(t)\rangle$, as shown in equations (21) and (22).

3.1.2. Orientational anisotropy during creep. In the creep process, the Rouse chains fully equilibrated at $t < 0$ are subjected to a constant stress σ_0 at $t \geqslant 0$. The equilibrium isotropic conformation, characterized with $\langle X_p Y_q\rangle_\mathrm{eq} = 0$, serves as the initial condition for equations (18) and (19). With this initial condition, equations (17)–(19) give the orientational anisotropy of the Rouse eigenmodes. The results are summarized as [10]

$$\langle X_p(t)Y_q(t)\rangle = \delta_{pq}\frac{2a^2 N}{3p^2\pi^2}\int_0^t \mathrm{d}t'\,\dot\gamma(t')\exp\left(-\frac{p^2(t-t')}{\tau_\mathrm{R}}\right). \tag{23}$$

The shear rate $\dot\gamma(t)$ included in this expression of $\langle X_p(t)Y_p(t)\rangle$ is self-consistently determined in such a way that the stress calculated from $\langle X_p(t)Y_p(t)\rangle$ coincides with the applied constant stress σ_0 (=σ_steady). That is, from equations (21)–(23) together with equation (11*b*) with $\sigma(t) = \sigma_0$ at $t > 0$, we obtain an integral equation for $\dot\gamma(t)$,

$$\sigma_0 = \nu k_\mathrm{B}T\sum_{p=1}^{\infty}\int_0^t \mathrm{d}t'\,\dot\gamma(t')\exp\left(-\frac{p^2(t-t')}{\tau_\mathrm{R}}\right). \tag{24}$$

This equation can be solved with the Laplace inversion method described in appendix A. The strain (integral of $\dot{\gamma}$) thus obtained is summarized as

$$\gamma(t) = \sigma_0 \left\{ \frac{t}{\eta_0} + J_r(t) \right\} \tag{25}$$

where η_0 and $J_r(t)$ are the zero-shear viscosity and recoverable compliance given by

$$\eta_0 = \frac{\nu k_B T \pi^2 \tau_R}{6} \tag{26}$$

and

$$J_r(t) = \frac{4}{\nu k_B T} \sum_{p=1}^{\infty} \frac{1}{\theta_p^2} \left\{ 1 - \exp\left(-\frac{t}{\lambda_p} \right) \right\} \qquad \text{with } \lambda_p = \frac{\pi^2 \tau_R}{\theta_p^2} \quad (p\text{th retardation time}). \tag{27}$$

The numerical coefficients θ_p appearing in equation (27) are determined from [10]

$$\tan\theta_p = \theta_p \qquad (p\pi < \theta_p < (p+1/2)\pi \text{ and } \theta_p \to (p+1/2)\pi \text{ for } p \to \infty). \tag{28}$$

These coefficients satisfy summation rules,

$$\sum_{q=1}^{\infty} \frac{1}{\theta_q^2} = \frac{1}{10}, \qquad \sum_{q=1}^{\infty} \frac{1}{p^2 - (\theta_q/\pi)^2} = -\frac{3}{2p^2}. \tag{29}$$

Substituting the shear rate $\dot{\gamma}(t)$ ($=\sigma_0\{\eta_0^{-1} + \dot{J}_r(t)\}$) calculated from equations (25)–(27) into equation (23), we obtain an explicit expression for the normalized anisotropy $A_p(t)$ of the pth Rouse eigenmode,

$$A_p(t) = \frac{2}{p^2\pi^2} + \frac{4}{3\pi^2} \sum_{q=1}^{\infty} \frac{1}{p^2 - (\theta_q/\pi)^2} \exp\left(-\frac{t}{\lambda_q} \right) \qquad \text{for creep process.} \tag{30}$$

Equations (21) and (30) specify the orientation function $S(n, t)$ of the monodisperse Rouse chains (in the continuous limit) during the creep process.

3.1.3. Orientational anisotropy during creep recovery. From equations (22) and (30), the eigenmode anisotropy in the steadily flowing state is given by $\langle X_p Y_q \rangle_{\text{steady}} = \delta_{pq}\{4\sigma_0 a^2 N/\nu k_B T p^4 \pi^4\}$ with $\sigma_0 = \sigma_{\text{steady}}$. Utilizing this $\langle X_p Y_q \rangle_{\text{steady}}$ as the initial condition for equations (18) and (19), we find the eigenmode anisotropy during the creep recovery from the steadily flowing state [10]:

$$\langle X_p(t) Y_q(t) \rangle = \delta_{pq} \frac{4\sigma_0 a^2 N}{\nu k_B T p^4 \pi^4} \exp\left(-\frac{p^2 t}{\tau_R} \right) + \delta_{pq} \frac{2a^2 N}{3p^2\pi^2} \int_0^t \mathrm{d}t' \, \dot{\gamma}(t') \exp\left(-\frac{p^2(t-t')}{\tau_R} \right). \tag{31}$$

Requiring the shear rate $\dot{\gamma}(t)$ included in equation (31) to satisfy the zero-stress condition during the recovery process (equations (21), (22), (31) together with equation (11b) with $\sigma(t) = 0$ at $t > 0$), we obtain an integral equation for $\dot{\gamma}(t)$,

$$0 = \sum_{p=1}^{\infty} \frac{6\sigma_0}{p^2\pi^2} \exp\left(-\frac{p^2 t}{\tau_R} \right) + \nu k_B T \sum_{p=1}^{\infty} \int_0^t \mathrm{d}t' \, \dot{\gamma}(t') \exp\left(-\frac{p^2(t-t')}{\tau_R} \right). \tag{32}$$

This equation is solved with the Laplace inversion method (appendix B) to give

$$\dot{\gamma}(t) = -\frac{4\sigma_0}{\nu k_B T \pi^2 \tau_R} \sum_{p=1}^{\infty} \exp\left(-\frac{t}{\lambda_p} \right) \qquad \text{with } \lambda_p = \frac{\pi^2 \tau_R}{\theta_p^2} \tag{33}$$

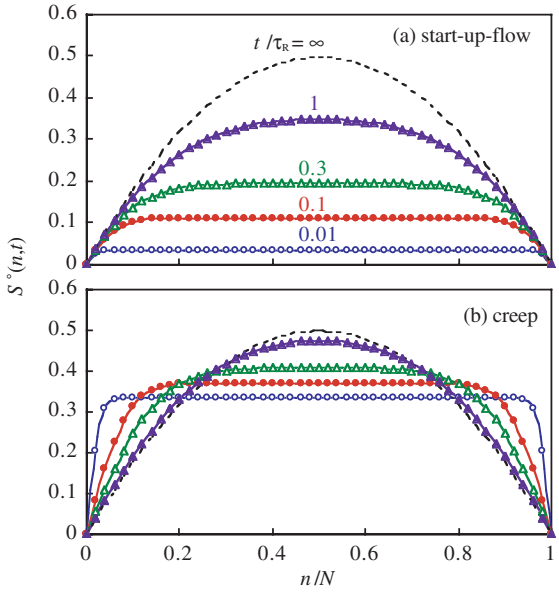

Figure 2. Growth of anisotropy along the chain backbone (a) after start-up of flow and (b) during the creep process. Symbols are the same in the top and bottom panels.

where θ_p is the coefficient specified by equation (28). Substituting this $\dot{\gamma}(t)$ into equation (31), we obtain the normalized anisotropy of the pth Rouse eigenmode, $A_p(t)$. The results are summarized as

$$A_p(t) = -\frac{4}{3\pi^2}\sum_{q=1}^{\infty}\frac{1}{p^2-(\theta_q/\pi)^2}\exp\left(-\frac{t}{\lambda_q}\right) \qquad \text{for creep recovery.} \quad (34)$$

3.1.4. Difference between stress-controlled and strain rate-controlled processes. Here, it is of interest to compare the evolution of the orientational anisotropy along the chain backbone under stress- and strain-controlled conditions. Under the latter condition, the shear rate $\dot{\gamma}(t)$ is externally given and the amplitudes of the Rouse eigenmodes, $X_p(t)$ and $Y_p(t)$, are straightforwardly calculated from equations (18) and (19) with appropriate initial conditions. The results for the start-up and cessation of constant rate flow can be summarized for the normalized anisotropy of the Rouse eigenmodes as [10]

$$A_p(t) = \frac{2}{p^2\pi^2}\left\{1-\exp\left(-\frac{p^2t}{\tau_R}\right)\right\} \qquad \text{after start-up of flow} \quad (35)$$

$$A_p(t) = \frac{2}{p^2\pi^2}\exp\left(-\frac{p^2t}{\tau_R}\right) \qquad \text{after cessation of steady flow.} \quad (36)$$

Here, τ_R is the longest viscoelastic Rouse relaxation time specified by equation (20).

Growth of the orientational anisotropy along the chain backbone is shown in figures 2(a) and (b) for the processes of start-up flow and creep, respectively. For the best comparison of these two processes, a normalized orientation function $S^\circ(n,t) = \{\nu(N-1)k_BT/\sigma_{steady}\}S(n,t)$ (with $\sigma_{steady} = \sigma_0$ in the creep process) calculated from equations (21), (30), and (35) is plotted against a normalized segment coordinate, n/N. (For $N \gg 1$, this plot does not change with N.)

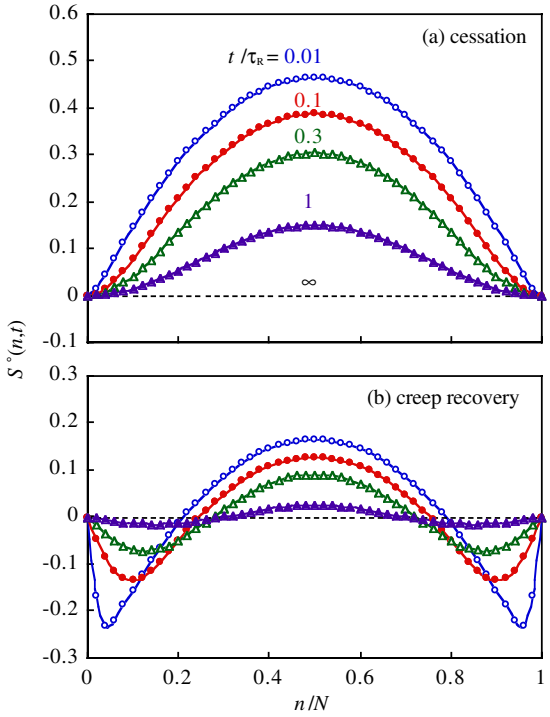

Figure 3. Decay of anisotropy along the chain backbone (a) after cessation of steady flow and (b) during creep recovery. Symbols are the same in the top and bottom panels.

Although the initial state (equilibrium state) and the steadily flowing state (at $t = \infty$) are common for the two processes, several important differences are observed in the transient state during these processes. We first note that the approach to the steady state ($S^\circ(n, \infty)$ shown with the dotted curve) is faster for the creep than for the start-up flow, because the longest retardation time $\lambda_1 = \pi^2\tau_R/\theta_1^2$ (=0.4888τ_R; evaluated from equation (28)) is considerably shorter than the longest relaxation time τ_R. We also note that $S^\circ(n, t)$ of all segments (all n values) monotonically increases to $S^\circ(n, \infty)$ during the start-up flow process. In contrast, during the creep process, $S^\circ(n, t)$ for the segments near the chain ends increase once above $S^\circ(n, \infty)$ and then decay to $S^\circ(n, \infty)$. This overshoot of the orientational anisotropy near the chain ends naturally results from the constant stress requirement during the creep process, as discussed later in more detail.

For the processes of cessation of steady flow and creep recovery, respectively, figures 3(a) and (b) show decay of the orientational anisotropy along the chain backbone. The normalized orientation function $S^\circ(n, t)$ calculated from equations (21), (34), and (36) is plotted against n/N. Although the initial, steadily flowing state and the final, isotropic state are common for the two processes, the decay of the anisotropy is faster in the creep recovery process than in the cessation process (because $\lambda_1 < \tau_R$). A more spectacular difference is noted for the segments near the chain ends during the creep recovery (figure 3(b)). These segments undershoot once to negative orientation (in the direction opposite to the steady flow direction at $t < 0$) and then approach the isotropic state. In contrast, after cessation of constant rate flow, all segments exhibit monotonic decay in their orientational anisotropy (figure 3(a)).

The overshoot and undershoot of the orientational anisotropy of the segments near the chain ends, seen in the creep and recovery processes, respectively, are natural consequences

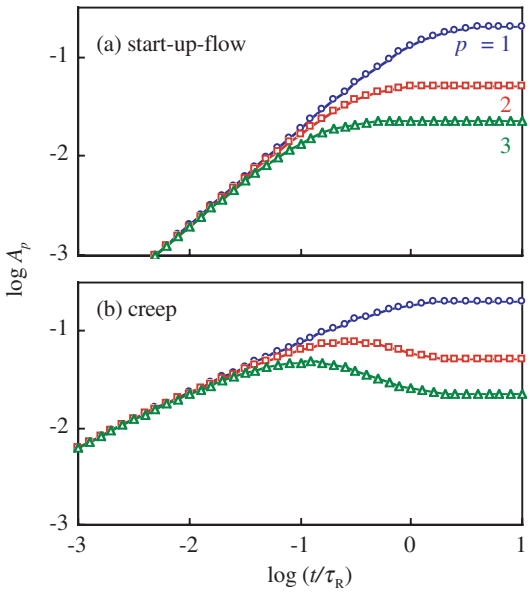

Figure 4. Growth of the normalized anisotropy A_p of Rouse eigenmodes with $p = 1$–3 (a) after start-up of flow and (b) during creep. Symbols are the same in the top and bottom panels. Reproduced, with permission, from [10].

of the constant stress requirement during these processes. In the creep process, the total anisotropy (the integral of $S(n, t)$ along the chain backbone; see equation (11*b*)) should match the applied, constant stress σ_0 at any $t > 0$. The segments near the ends can change their orientation more rapidly than those at the chain centre, because the motion near the ends is more significantly contributed from higher order Rouse eigenmodes compared to the motion at the centre (as can be noted from the $\sin^2(p\pi n/N)$ factor for $S(n, t)$ shown in equation (21); this factor is larger for larger p at $n \simeq 0$ and N). These quickly moving segments near the chain ends are forced to be over-orientated at short t so as to *compensate* a slow growth of the orientation at the centre. At long t where the chain centre has adjusted its conformation to have a large anisotropy, the segments near the ends are no longer forced to make this compensation and thus becomes less orientated (because the chain end itself serves as a source of isotropic conformation; this role of the chain end is represented through the boundary condition for the Rouse motion, equation (8)). The overshoot of the orientation near the chain ends occurs in this way. Similarly, the negative undershoot near the chain ends during the recovery process results from the compensation of the slowly decaying positive orientation at the chain centre under the zero-stress condition.

In the strain-controlled processes of start-up and cessation of constant rate flow, the anisotropy of the segments near the chain ends exhibits no overshoot/undershoot and rapidly approaches its steady state (figures 2(a) and 3(a)). This behaviour reflects the lack of the constant stress requirement during these processes.

For further investigation of the effect of this requirement on each Rouse eigenmode, figure 4 compares the normalized anisotropies A_p of the first to third eigenmodes ($p = 1$–3) during the start-up flow and creep processes (see equations (30) and (35)). Figure 5 makes the comparison of A_p for the cessation and creep recovery processes (see equations (34) and (36)). In both figures, A_p (or $|A_p|$) is double-logarithmically plotted against a normalized time, t/τ_R.

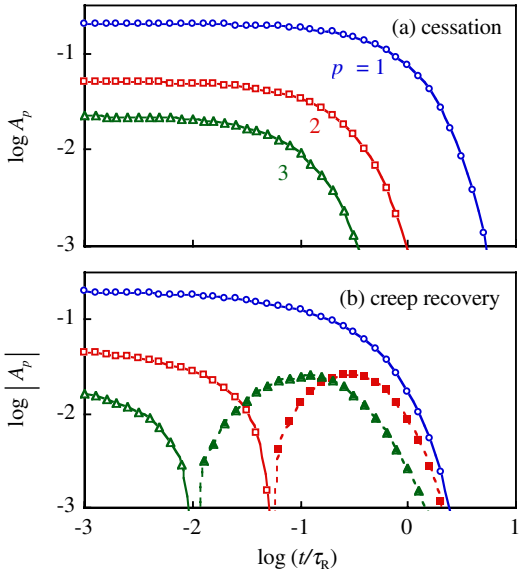

Figure 5. Decay of the normalized anisotropy A_p of Rouse eigenmodes with $p = 1$–3 (a) after cessation of flow and (b) during creep recovery. Unfilled and filled symbols indicate positive and negative A_p values. Symbols are the same in the top and bottom panels. Reproduced, with permission, from [10].

After start-up of flow, A_p of each Rouse eigenmode is governed by a single characteristic time τ_R/p^2 (see equation (35)) and exponentially approaches its steady state, as seen in figure 4(a). This single Voigt behaviour indicates that the Rouse eigenmodes of different orders behave independently under the rate-controlled flow.

In contrast, in the stress-controlled creep process, A_1 for the lowest Rouse eigenmode monotonically increases to its steady state value while A_2 and A_3 for the second and third eigenmodes exhibit an overshoot before attaining their steady state, as seen in figure 4(b). Similar overshoot is found for all higher eigenmodes (with $p \geqslant 4$). The non-Voigt behaviour of the Rouse eigenmodes, characterized with this overshoot, results from the constant stress requirement, $\sum_{p=1}^{\infty} A_p(t) = 1/3$ (derived from equations (11*b*) and (21) with $\sigma(t) = \sigma_0 = \sigma_{\text{steady}}$). Because of this requirement, the Rouse eigenmodes of different orders have interplay (or correlation) in their anisotropies so that the higher eigenmodes are forced to compensate the slow growth of A_1 of the lowest eigenmode. The overshoot of A_p of the higher eigenmodes (figure 4(b)), leading to the overshoot of $S^\circ(n, t)$ near the chain ends (figure 2(b)), is a natural consequence of this compensation.

An even more striking difference is observed for the eigenmode anisotropies A_p in the processes of cessation of steady flow and creep recovery. After cessation of flow, all Rouse eigenmodes behave independently so that their A_p (equation (36)) exhibit monotonic exponential decay, as observed in figure 5(a). In contrast, in the creep recovery process, the eigenmodes of different orders exhibit an interplay in order to satisfy the zero-stress requirement, $\sum_{p=1}^{\infty} A_p(t) = 0$ (see equations (11*b*) and (21) with $\sigma(t) = 0$). Because of this requirement, the A_p for the higher eigenmodes undershoot to negative values (shown in figure 5(b) with filled symbols connected with dotted curves) in order to compensate a slow decay of positive A_1 of the lowest eigenmode. The undershoot of $S^\circ(n, t)$ near the chain ends during the creep recovery (figure 3(b)) reflects this undershoot of A_p of the higher eigenmodes.

3.2. Binary blends of Rouse chains with $N \gg 1$ [11]

We have seen that the Rouse eigenmodes of monodisperse chains (with $N \gg 1$) exhibit non-Voigt behaviour during the creep/recovery processes because of their interplay due to the constant stress requirement. For binary blends of short and long Rouse chains, we expect similar interplay between the component chains having different relaxation times. This section examines the orientational anisotropies of these component chains during the creep process.

3.2.1. Anisotropy in blends. We consider binary blends of short and long Rouse chains (component chains 1 and 2) each composed of N_1 and N_2 segments. For the component chain j, the weight fraction is denoted as w_j and the number density is given by $\nu_j = (w_j/N_j)/\{(w_1/N_1) + (w_2/N_2)\}$.

In the blends, each component chain obeys the Rouse equation of motion. We assume $N_2 > N_1 \gg 1$ so that the component dynamics is described by the continuous version of the equation of motion, equation (6). Then, the position of the segments of each component is expressed in terms of the Rouse eigenmodes in the form of equation (12). The amplitudes of the pth eigenmode of the component j in the shear and shear gradient directions, $X_p^{[j]}(t)$ and $Y_p^{[j]}(t)$, obey the time evolution equations (14) and (15) and their time-dependent changes are described by equations (18) and (19). The corresponding orientational anisotropy of the Rouse eigenmodes, $\langle X_p^{[j]}(t) Y_p^{[j]}(t)\rangle$, is determined by the integral equation (23) with N and τ_R therein being replaced by N_j and $\tau_R^{[j]}$ ($=\zeta N_j^2 a^2/6\pi^2 k_B T$; longest relaxation time of the component j), respectively. The shear rate $\dot\gamma(t)$ included in this integral equation is determined from the constant stress requirement, $\sigma(t) =$ applied stress σ_0. In the blends, the stress is sustained by both of the components 1 and 2, and this requirement is written as [11]

$$\sigma_0 = k_B T \int_0^t dt'\, \dot\gamma(t') \left\{ \nu_1 \sum_{p=1}^{\infty} \exp\left(-\frac{p^2(t-t')}{\tau_R^{[1]}}\right) + \nu_2 \sum_{p=1}^{\infty} \exp\left(-\frac{p^2(t-t')}{\tau_R^{[2]}}\right) \right\}. \tag{37}$$

(For monodisperse systems, equation (37) reduces to equation (24).)

Equation (37) can be solved with a Laplace inversion method similar to that described in appendix A. The shear rate thus obtained is written as [11]

$$\dot\gamma(t) = \sigma_0 \left\{ \frac{1}{\eta_0} + \frac{4}{\nu_1 k_B T \pi^2 \tau_R^{[1]}} \sum_{p=1}^{\infty} \frac{\Theta_p^2}{h_p} \exp\left(-\frac{t}{\Lambda_p}\right) \right\} \qquad \text{with } \Lambda_p = \frac{\pi^2 \tau_R^{[1]}}{\Theta_p^2} \tag{38}$$

with

$$\eta_0 = \frac{\pi^2 k_B T}{6}\left(\nu_1 \tau_R^{[1]} + \nu_2 \tau_R^{[2]}\right) \qquad \text{(viscosity of the blend)} \tag{39}$$

and

$$\begin{aligned} h_p = {} & \Theta_p^2 - (1 - \Theta_p \cot\Theta_p)(1 + \Theta_p \cot\Theta_p) \\ & + \frac{\nu_2}{\nu_1}\left[\left(\frac{N_2\Theta_p}{N_1}\right)^2 - \left\{ 1 - \left(\frac{N_2\Theta_p}{N_1}\right) \cot\left(\frac{N_2\Theta_p}{N_1}\right) \right\} \right. \\ & \left. \times \left\{ 1 + \left(\frac{N_2\Theta_p}{N_1}\right) \cot\left(\frac{N_2\Theta_p}{N_1}\right) \right\} \right]. \end{aligned} \tag{40}$$

The coefficients Θ_p appearing in equations (38) and (40) are determined from

$$\nu_1 \{\Theta_p \cot\Theta_p - 1\} + \nu_2 \left\{ \left(\frac{N_2\Theta_p}{N_1}\right) \cot\left(\frac{N_2\Theta_p}{N_1}\right) - 1 \right\} = 0. \tag{41}$$

For $\nu_2 = 0$ and/or $N_2 = N_1$ (i.e., for monodisperse systems), Θ_p reduces to θ_p specified by equation (28) and h_p coincides with θ_p^2.

Utilizing the shear rate $\dot{\gamma}(t)$ given by equation (38) in (23) (with $N = N_j$ and $\tau_R = \tau_R^{[j]}$), we can calculate the orientational anisotropy of the Rouse eigenmodes, $\langle X_p^{[j]}(t) Y_p^{[j]}(t)\rangle$. The result is conveniently written for the normalized anisotropy of the pth eigenmode [11],

$$A_p^{[j]}(t) \equiv \frac{\nu_j k_B T p^2 \pi^2}{2\sigma_0 a^2 N_j} \langle X_p^{[j]}(t) Y_p^{[j]}(t)\rangle = \frac{2\nu_j N_j^2}{p^2\pi^2(\nu_1 N_1^2 + \nu_2 N_2^2)} + \frac{4\nu_j}{3\pi^2\nu_1} \sum_{q=1}^{\infty} \frac{\Theta_q^2}{h_q\{(pN_1/N_j)^2 - (\Theta_q/\pi)^2\}} \exp\left(-\frac{t}{\Lambda_q}\right). \tag{42}$$

The stresses $\sigma^{[j]}$ sustained by the short and long chains ($j = 1$ and 2), representing the conformational anisotropies summed over the backbones of these chains, are expressed in terms of these $A_p^{[j]}(t)$ as

$$\sigma^{[j]} = 3\sigma_0 \sum_{p=1}^{\infty} A_p^{[j]}(t). \tag{43}$$

3.2.2. Interplay between short and long chains in blend. For the blends having $N_2/N_1 = 3$ and 10, figure 6(a) shows growth of the stress $\sigma^{[j]}(t)$ sustained by the short and long chains during the creep process (equations (42) and (43)). The weight fractions of these chains are $w_1 = w_2 = 0.5$. For comparison, the growth in the monodisperse system ($N_2/N_1 = 1$) is also shown. For the clearest comparison of the behaviour in the blends and the monodisperse system, $\sigma^{[j]}(t)$ is normalized by $\sigma_0 w_j$ and semi-logarithmically plotted against a normalized time defined for the short chain, $t/\tau_R^{[1]}$.

After start-up of the constant rate flow (without the constant stress requirement), the component chains in the blends behave independently. Thus, the normalized stress $\sigma^{[j]}(t)/\sigma_0 w_j$ of the component j after start-up of flow is identical to that in the monodisperse system. From equations (35) and (43), this stress is obtained as

$$\frac{\sigma^{[j]}}{\sigma_0 w_j} = \frac{(1/N_j)}{(w_1/N_1) + (w_2/N_2)} \frac{k_B T \tau_R^{[j]}}{\eta_0} \sum_{p=1}^{\infty} \frac{1}{p^2} \left\{1 - \exp\left(-\frac{p^2 t}{\tau_R^{[j]}}\right)\right\} \tag{44}$$

where η_0 is the blend viscosity given by equation (39). Figure 6(b) shows plots of this $\sigma^{[j]}(t)/\sigma_0 w_j$.

The steady state is the same for the creep and start-up flow processes, and the ratio of the steady stresses of the long and short chains, $\sigma^{[2]}(\infty)/\sigma^{[1]}(\infty)$, increases with the N_2/N_1 ratio. Specifically, $\sigma^{[2]}(\infty)/\sigma^{[1]}(\infty) = (\tau_R^{[2]}/N_2)/(\tau_R^{[1]}/N_1) = N_2/N_1$ for $w_2 = w_1$ (see equation (44)). However, this increase merely reflects a distribution of the total stress $\sigma^{[2]}(\infty) + \sigma^{[1]}(\infty)$ for the short and long chains having different relaxation times $\tau_R^{[1]}$ and $\tau_R^{[2]}$.

The essential feature under the rate-controlled flow is the *independent* stress growth of the short and long chains that reflects independent conformational evolution of these chains. This feature is observed in figure 6(b) as a coincidence of a fractional stress $\sigma^{[1]}(t)/\sigma^{[1]}(\infty)$ of the short chain in the blends and monodisperse system at *any* t. (In figure 6(b), $\sigma^{[2]}(t)$ for the long chain is plotted against the normalized time for the short chain, $t/\tau_R^{[1]}$, and thus the growth of $\sigma^{[2]}(t)$ looks delayed with increasing N_2/N_1 ratio. However, this superficial delay vanishes when $\sigma^{[2]}(t)$ is plotted against the normalized time for the long chain $t/\tau_R^{[2]}$, as clearly noted from equation (44).)

In contrast, during the creep process, the stresses $\sigma^{[1]}(t)$ and $\sigma^{[2]}(t)$ of the short and long chains synchronously decay and grow, respectively, in such a way that the total stress

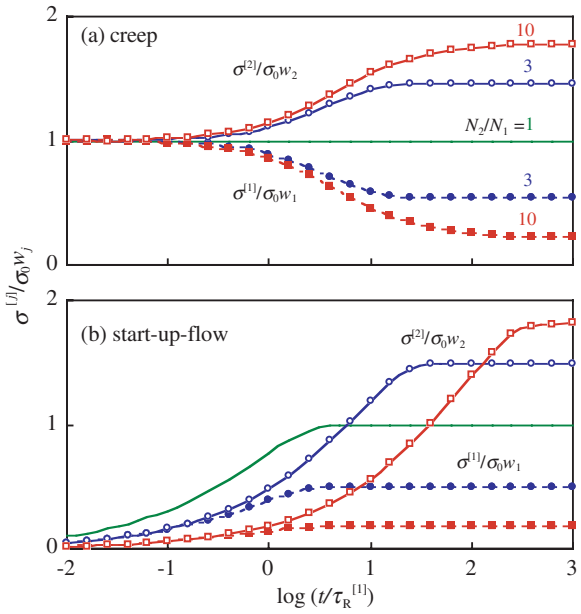

Figure 6. Normalized stress sustained by the short and long Rouse chains ($j = 1$ and 2) in the blends with $w_1 = w_2 = 0.5$ and N_2/N_1 as indicated. The stresses (a) during the creep process and (b) after start-up of constant rate flow are plotted against the normalized time for the short chain, $t/\tau_R^{[1]}$. Symbols are the same in the top and bottom panels. Reproduced, with permission, from [11].

$\sigma^{[1]}(t) + \sigma^{[2]}(t)$ is kept constant ($=\sigma_0$); see figure 6(a). Consequently, a time $t_s^{[1]}$ required for achieving the steady state for the short chain increases with increasing N_2, because the conformational change of the long chain determining the growth of $\sigma^{[2]}(t)$ becomes slower for larger N_2 and the short chain having a much shorter relaxation time ($\tau_R^{[1]}$) is forced to compensate this slow growth. These features of the creep process demonstrate the importance of the conformational interplay (correlation) of the short and long chains under the constant stress requirement.

The eigenmodes of respective chains also exhibit the interplay, as demonstrated in figures 7 and 8 where the eigenmode anisotropies $A_p^{[j]}$ ($p = 1$–3; equation (42)) of the component chain j in the blends are normalized by the weight fractions w_j and double-logarithmically plotted against a normalized time $t/\tau_R^{[j]}$.

As seen in the top panel of figure 7, $A_1^{[2]}$ for the lowest eigenmode of the long chain increases monotonically with t. The anisotropies of the higher eigenmodes, $A_2^{[2]}$ and $A_3^{[2]}$, overshoot before attaining their steady state, thereby compensating the slow growth of $A_1^{[2]}$, as observed in the middle and bottom panels. This overshoot is indicative of the interplay of the eigenmodes during the creep process, as discussed earlier for monodisperse systems. It should also be noted that the monotonic growth of $A_1^{[2]}$ and the overshoot of $A_2^{[2]}$ and $A_3^{[2]}$ are qualitatively similar in the monodisperse system ($N_2/N_1 = 1$; curves without symbol) and the blends (circle and triangle). That is, the interplay among the eigenmodes of the long chain is just moderately affected by blending.

In contrast, for the short chain in the blend, the overshoot of the higher eigenmodes ($p = 2$ and 3) is quite prominent (compared to that for the long chain) and even the lowest eigenmode

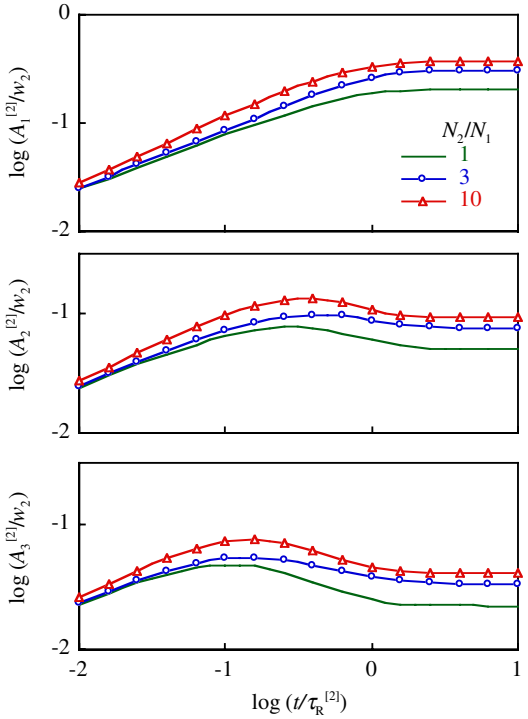

Figure 7. Anisotropies $A_p^{[2]}$ of the first to third Rouse eigenmodes of the long chain in the blends with $w_1 = w_2 = 0.5$ and N_2/N_1 as indicated. $A_p^{[2]}$ is normalized by w_2 and plotted against the normalized time for the long chain, $t/\tau_R^{[2]}$. Symbols are the same in all panels. Reproduced, with permission, from [11].

exhibits the overshoot, as demonstrated in figure 8. This result indicates that all eigenmodes of the short chain can adjust themselves quickly compared to the eigenmodes of the long chain, thereby compensating the slow growth of the latter. Thus, the eigenmodes of the short chain are strongly affected by the orientational interplay between the long and short chains during the creep process.

3.3. Monodisperse Rouse chains with small N [13]

The continuous version of the Rouse model (equation (6)) is applicable to a real chain in a timescale not very much shorter than the longest relaxation time τ_1 of this chain. However, this model gives an infinite number of retardation modes and the retardation time λ_p approaches zero with increasing mode index $p \to \infty$ (see equations (27) and (28)). This feature is an artefact of the continuous model, and the fast dynamics of the real chain (having a finite number of modes with $\lambda_p > 0$) cannot be described by this model. A corresponding artefact is well known for the relaxation modulus $G(t)$: the continuous model gives an infinitely large instantaneous modulus $G(0)$ while the real chain has a finite value of $G(0)$.

Thus, for description of the behaviour of the real chain over the entire range of time (including the short timescale), we have to utilize a discrete Rouse chain composed of a finite number of beads and having a finite number of retardation modes. Obviously, all retardation times λ_p of the discrete chain are positive, and it takes a finite time for the chain to exhibit

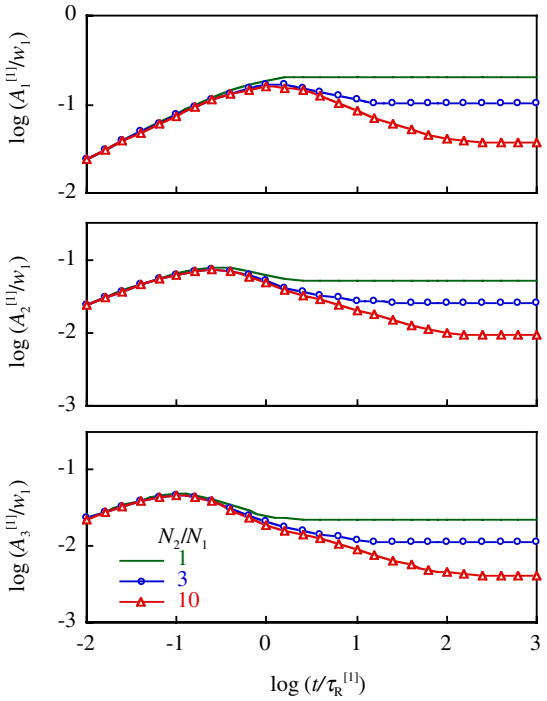

Figure 8. Anisotropies $A_p^{[1]}$ of the first to third Rouse eigenmodes of the short chain in the blends with $w_1 = w_2 = 0.5$ and N_2/N_1 as indicated. $A_p^{[1]}$ is normalized by w_1 and plotted against the normalized time for the short chain, $t/\tau_R^{[1]}$. Symbols are the same in all panels. Reproduced, with permission, from [11].

the retardational motion. Concerning this feature of the discrete chain, we naturally ask a question: How does this chain abruptly change its conformation on imposition/removal of the stress during the creep/recovery processes? For this question, an analysis of the discrete chain conformation during these processes is highly desired. (Surprisingly, neither results of this analysis nor related experimental data are found in the literature.)

As the simplest but still informative model cases, we recently analysed the conformational changes of discrete, monodisperse Rouse chains with the segment (bead) number $N = 3$ and 4 [13]. The analysis revealed that the chain is *affinely* deformed (without being contributed from the retardation modes) on abrupt imposition/removal of the stress and this deformation determines the instantaneous value of the recoverable compliance. Details of this behaviour are explained below.

3.3.1. Four-bead Rouse chain. For the monodisperse Rouse chain composed of four beads ($N = 4$), the discrete version of the equation of motion utilizing a 4×4 Rouse matrix (see equations (3) and (4)) can be easily solved by expanding the segment position with respect to four discrete Rouse eigenmodes [13]. The zeroth eigenmode is related to the centre-of-mass diffusion, and the internal eigenmodes (first to third eigenmodes) represent conformational changes of the chain. The relaxation times of these internal eigenmodes are given by

$$\tau_1 = \frac{(2+\sqrt{2})\varsigma}{4\kappa}, \qquad \tau_2 = \frac{\varsigma}{4\kappa}, \qquad \tau_3 = \frac{(2-\sqrt{2})\varsigma}{4\kappa} \tag{45}$$

where ζ and κ are the friction coefficient of the bead (segment) and the spring constant, respectively (see figure 1). During the creep under a constant stress σ_0, the four-bead Rouse chain itself determines the shear rate $\dot{\gamma}(t)$ in such a way that its stress matches the applied stress. Specifically, $\dot{\gamma}(t)$ is determined by an integral equation (similar to equation (24) for the case of $N \to \infty$),

$$\sigma_0 = \nu k_B T \int_0^t dt' \, \dot{\gamma}(t') \sum_{p=1}^{3} \exp\left(-\frac{t-t'}{\tau_p}\right) \qquad \text{for creep of four-bead chain} \tag{46}$$

where ν is the chain number density. This equation is solved to give the creep compliance $J(t)$ $(=\gamma(t)/\sigma_0)$ [13],

$$J(t) = \frac{t}{\eta_0} + J_r(t) \qquad \text{with viscosity } \eta_0 = \frac{5\nu k_B T \zeta}{4\kappa}. \tag{47}$$

The recoverable compliance $J_r(t)$ is written as

$$J_r(t) = \frac{1}{3\nu k_B T}\left[1 + \frac{7+2\sqrt{6}}{25}\left\{1 - \exp\left(-\frac{t}{\lambda_1}\right)\right\} + \frac{7-2\sqrt{6}}{25}\left\{1 - \exp\left(-\frac{t}{\lambda_2}\right)\right\}\right] \tag{48}$$

with retardation times being given by

$$\lambda_1 = \frac{(6+\sqrt{6})\zeta}{20\kappa}, \qquad \lambda_2 = \frac{(6-\sqrt{6})\zeta}{20\kappa}. \tag{49}$$

The orientational anisotropy $\langle X_p(t) Y_p(t)\rangle$ of the pth Rouse eigenmode ($p = 1$–3) is calculated from the shear rate $\dot{\gamma}(t)(=\dot{J}(t)\sigma_0)$ through an integral equation similar to equation (23). $\langle X_p(t) Y_p(t)\rangle$ for each eigenmode has a distribution in the retardation times, and each retardation mode is contributed from the first to third Rouse eigenmodes. This fact can be most clearly demonstrated for the stress $\sigma_p(t)$ sustained by the pth eigenmode $(\sigma_p(t) \propto \langle X_p Y_p\rangle)$,

$$\sigma_1(t) = \sigma_0\left\{\frac{2+\sqrt{2}}{5} - \frac{(\sqrt{6}+1)(\sqrt{3}+1)}{30}\exp\left(-\frac{t}{\lambda_1}\right) - \frac{(\sqrt{6}-1)(\sqrt{3}-1)}{30}\exp\left(-\frac{t}{\lambda_2}\right)\right\} \tag{50a}$$

$$\sigma_2(t) = \sigma_0\left\{\frac{1}{5} + \frac{\sqrt{6}+1}{15}\exp\left(-\frac{t}{\lambda_1}\right) - \frac{\sqrt{6}-1}{15}\exp\left(-\frac{t}{\lambda_2}\right)\right\} \tag{50b}$$

$$\sigma_3(t) = \sigma_0\left\{\frac{2-\sqrt{2}}{5} + \frac{(\sqrt{6}+1)(\sqrt{3}-1)}{30}\exp\left(-\frac{t}{\lambda_1}\right) + \frac{(\sqrt{6}-1)(\sqrt{3}+1)}{30}\exp\left(-\frac{t}{\lambda_2}\right)\right\}. \tag{50c}$$

Of course, the sum $\sum_{p=1}^{3} \sigma_p(t)$ coincides with σ_0 at any t.

The orientation function $S(n,t)$ of the bond vector $\mathbf{u}(n,t)$ (defined by equations (9) and (10a)) is calculated from the anisotropies $\langle X_p(t) Y_p(t)\rangle$. The results can be summarized as

$$S(1,t) = S(3,t) = \frac{\sigma_0}{90\nu k_B T}\left\{9 + \frac{\sqrt{6}+1}{2}\exp\left(-\frac{t}{\lambda_1}\right) - \frac{\sqrt{6}-1}{2}\exp\left(-\frac{t}{\lambda_2}\right)\right\} \tag{51a}$$

$$S(2,t) = \frac{\sigma_0}{45\nu k_B T}\left\{6 - \frac{\sqrt{6}+1}{2}\exp\left(-\frac{t}{\lambda_1}\right) + \frac{\sqrt{6}-1}{2}\exp\left(-\frac{t}{\lambda_2}\right)\right\}. \tag{51b}$$

This $S(n,t)$ specifies the orientational anisotropy of respective bond vectors but does not represent an orientational cross-correlation of different bond vectors characterized by a

correlation function $S_c(n,m,t) = a^{-2}\langle u_x(n,t)u_y(m,t)\rangle_{n\neq m}$. This cross-correlation is reflected in an orientation function of the end-to-end vector $\mathbf{R} = \sum_{n=1}^{N-1}\mathbf{u}(n,t)$ defined by

$$S_R(t) \equiv \frac{\langle R_x(t)R_y(t)\rangle}{\langle R^2\rangle_{\rm eq}} = \frac{1}{N-1}\left\{\sum_{n=1}^{N-1} S(n,t) + \sum_{n,m(\neq n)=1}^{N-1} S_c(n,m,t)\right\}. \quad (52)$$

Here, $\langle R^2\rangle_{\rm eq}$ $(=(N-1)a^2)$ is the mean square end-to-end distance at equilibrium. For the four-bead chain, $S_R(t)$ is calculated from $\langle X_p(t)Y_p(t)\rangle$ as

$$S_R(t) = \frac{\sigma_0}{18\nu k_{\rm B}T}\left\{4 - \frac{3+\sqrt{6}}{3}\exp\left(-\frac{t}{\lambda_1}\right) - \frac{3-\sqrt{6}}{3}\exp\left(-\frac{t}{\lambda_2}\right)\right\}. \quad (53)$$

The stress $\sigma_p(t)$ for the pth eigenmode and the orientation functions $S(n,t)$ and $S_R(t)$ during the creep recovery process are related to those during the creep process (equations (50), (51), and (53)) as

$$[\sigma_p(t)]_{\rm recovery} = [\sigma_p(\infty)]_{\rm creep} - [\sigma_p(t)]_{\rm creep} \quad (54)$$

$$[S(n,t)]_{\rm recovery} = [S(n,\infty)]_{\rm creep} - [S(n,t)]_{\rm creep} \quad (55)$$

$$[S_R(t)]_{\rm recovery} = [S_R(\infty)]_{\rm creep} - [S_R(t)]_{\rm creep}. \quad (56)$$

3.3.2. Three-bead Rouse chain. The three-bead chain has two (first and second) internal eigenmodes describing the chain conformation. The anisotropies $\langle X_p(t)Y_p(t)\rangle$ of these eigenmodes, calculated with the method applied for the four-bead chain, give the stress $\sigma_p(t)$ for the pth eigenmode, the orientation functions $S(n,t)$ $(n=1,2)$ and $S_R(t)$, and the recoverable compliance $J_{\rm r}(t)$:

$$\sigma_1(t) = \sigma_0\left\{\frac{3}{4} - \frac{1}{4}\exp\left(-\frac{t}{\lambda_1}\right)\right\}, \qquad \sigma_2(t) = \sigma_0\left\{\frac{1}{4} + \frac{1}{4}\exp\left(-\frac{t}{\lambda_1}\right)\right\} \quad (57)$$

$$S(1,t) = S(2,t) = \frac{\sigma_0}{6\nu k_{\rm B}T} \quad (t\text{-independent}),$$

$$S_R(t) = \frac{\sigma_0}{12\nu k_{\rm B}T}\left\{3 - \exp\left(-\frac{t}{\lambda_1}\right)\right\} \quad (58)$$

$$J_{\rm r}(t) = \frac{1}{2\nu k_{\rm B}T}\left[1 + \frac{1}{4}\left\{1 - \exp\left(-\frac{t}{\lambda_1}\right)\right\}\right]. \quad (59)$$

The single retardation time of the three-bead chain, λ_1, is related to the longest relaxation time τ_1 as

$$\lambda_1 = \frac{\tau_1}{2} = \frac{\zeta}{4\kappa}. \quad (60)$$

Equations (54)–(56) hold for $\sigma_p(t)$, $S(n,t)$, and $S_R(t)$ during the creep recovery process.

3.3.3. Crossover from affine to non-affine deformation. For the four-bead Rouse chain during the creep/recovery process, figure 9(a) shows plots of the normalized stress sustained by the pth eigenmode, $\sigma_p(t)/\sigma_0$ (equation (50)) against the normalized time t/τ_1. This chain has the instantaneous modulus $G(0) = \nu(N-1)k_{\rm B}T = 3\nu k_{\rm B}T$, and the corresponding instantaneous strain against the applied stress σ_0 is given by $\gamma_\sigma = \sigma_0/G(0) = \sigma_0/3\nu k_{\rm B}T$. The orientation functions normalized by this strain, $S^\circ(n,t) = S(n,t)/\gamma_\sigma$ and $S_R^\circ(t) = S_R(t)/\gamma_\sigma$, are shown in figure 9(b). For the three-bead chain, figure 10 shows $\sigma_p(t)/\sigma_0$, $S^\circ(n,t)$, and $S_R^\circ(t)$, with the normalizing strain for the latter two being given by $\gamma_\sigma = \sigma_0/2\nu N k_{\rm B}T$. In all panels of figures 9 and 10, the left and right halves indicate the time evolution of the quantities during the creep process and successive recovery process, respectively.

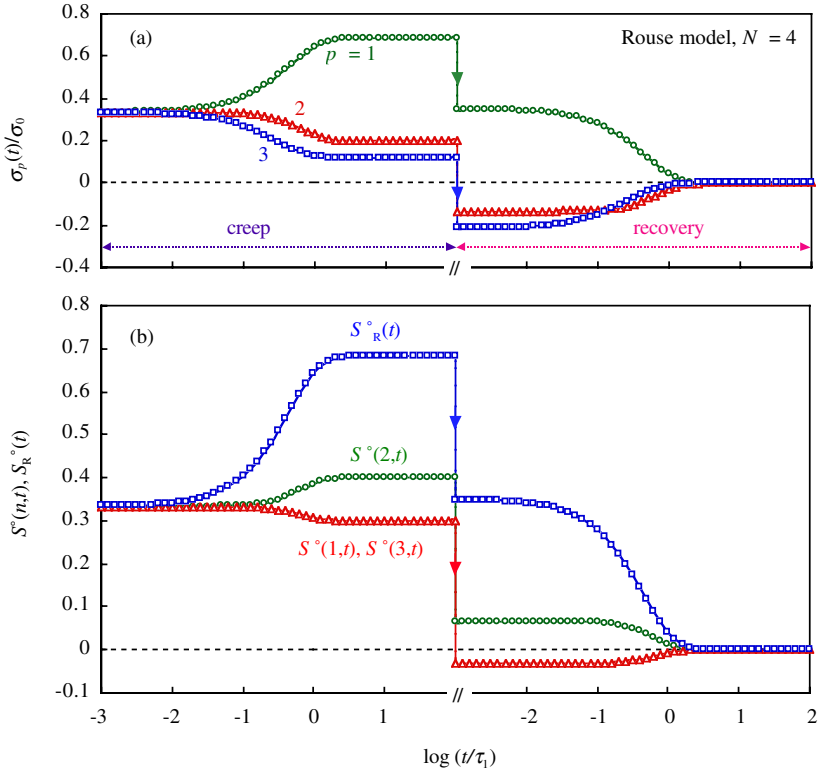

Figure 9. Creep and recovery behaviour of the four-bead Rouse chain; (a) normalized stress $\sigma_p(t)/\sigma_0$ sustained by the pth eigenmode, (b) normalized orientation functions $S^\circ(n,t)$ and $S^\circ_R(t)$ of the bond vectors and end-to-end vector. These quantities are plotted against the normalized time, t/τ_1.

We first focus on the creep behaviour of the four-bead and three-bead chains. All eigenmodes sustain the same, positive stress $\sigma_p(0) = \sigma_0/(N-1)$ at the onset of creep, as seen from figures 9(a) and 10(a) and equations (50) and (57). In this initial stage, the chain is uniformly orientated along its backbone to have an n-independent $S^\circ(n,0)$ value $(=\sigma_0/3(N-1)\nu k_B T\gamma_\sigma = 1/3)$; see figures 9(b) and 10(b) and equations (51) and (58). This uniform orientation corresponds to the *affine deformation* from the isotropic, equilibrium state by the magnitude of γ_σ, as explained in more detail in appendix C. The end-to-end vector is also affinely deformed at $t = 0$ to have $S_R(0) = \gamma_\sigma/3$; see equations (53) and (58) and appendix C.

The affine deformation of the chain is an instantaneous, elastic deformation against the modulus $G(0)$ and is not contributed from any retardation mode. For this reason, the affine deformation does occur instantaneously for the discrete Rouse chains having finite (non-zero) retardation times, thereby allowing this chain to adjust its conformation on imposition of the stress. It should be also noted that the instantaneous value of the recoverable compliance, $J_r(0) = 1/\nu(N-1)k_B T = 1/G(0)$ (equations (48) and (59)), is determined by this affine deformation.

After the initial stage, the stress $\sigma_1(t)$ sustained by the lowest eigenmode increases while $\sigma_2(t)$ and $\sigma_3(t)$ for the higher eigenmodes decrease with t to reach the respective steady states, as seen in figures 9(a) and 10(a). These transient changes of $\sigma_p(t)$ result from the interplay of

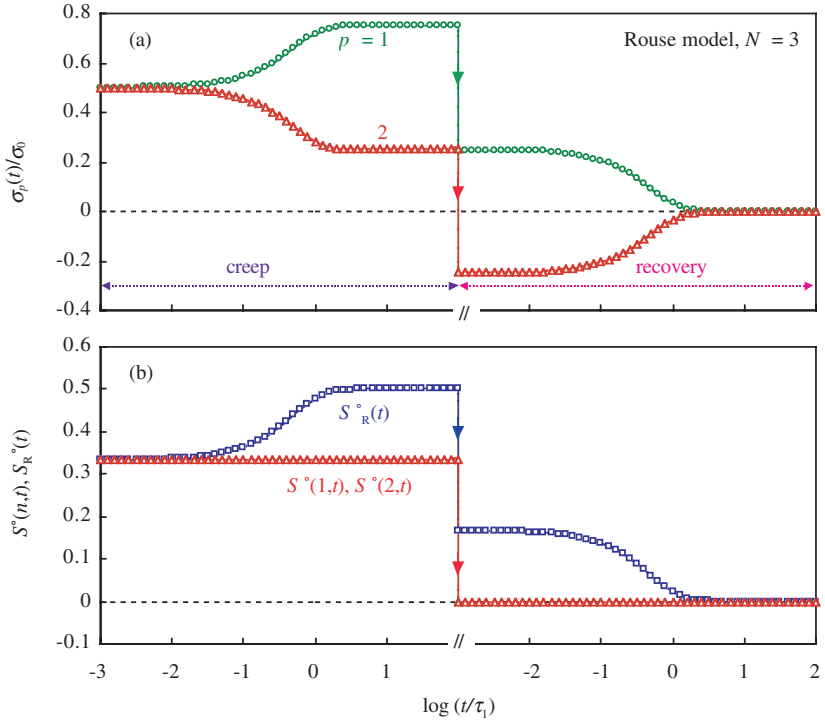

Figure 10. Creep and recovery behaviour of three-bead Rouse chain; (a) normalized stress $\sigma_p(t)/\sigma_0$ sustained by the pth eigenmode, (b) normalized orientation functions $S^{\circ}(n,t)$ and $S^{\circ}_R(t)$ of the bond vectors and end-to-end vector. These quantities are plotted against the normalized time, t/τ_1.

the eigenmodes under the constant stress requirement, as discussed earlier for the continuous chain: the $\sigma_p(t)$ for the fast, higher eigenmodes are forced to compensate a slow growth of $\sigma_1(t)$ for the lowest eigenmode and are allowed to decay to their steady state values only at long t.

For the four-bead chain, these transient changes of $\sigma_p(t)$ are associated with the increase of the orientational anisotropy of the bond vector at the middle of the chain ($S(2,t)$) and the decrease of the anisotropy of the bond vectors at the ends ($S(1,t)$ and $S(3,t)$), as seen in figure 9(b). This evolution of anisotropy is indicative of a conformational change from the initial affine state to the non-uniformly (*non-affinely*) oriented, steadily flowing state.

This evolution of anisotropy reflects the interplay between the quickly moving end vectors and slowly moving middle vector under the constant stress requirement, as discussed for the continuous chain. The non-instantaneous part of the $J_r(t)$ of the four-bead chain, shown by the $\{1-\exp(-t/\lambda_p)\}$ terms in equation (48), is contributed from the evolution of the anisotropy of the bond vectors (as well as from the evolution of cross-correlation explained below).

The situation is somewhat different for the three-bead chain. This chain has only two bond vectors. These vectors are equivalent to each other and thus have $S(1,t) = S(2,t)$ at any t. For this reason, $S(1,t)$ and $S(2,t)$ keep their initial values ($=\gamma_\sigma/3$) throughout the creep process, as noted in figure 10(b) and equation (58). However, the chain conformation itself exhibits a transient change to the steadily flowing state, as demonstrated by the growth of $S_R(t)$ of the end-to-end vector. This growth is associated with transient changes of σ_1 and

σ_2 (figure 10(a)) that are indicative of the interplay of all (two) eigenmodes under the constant stress requirement.

The growth of $S_R(t)$ of the three-bead chain is exclusively attributed to a growth of the orientational cross-correlation of neighbouring bond vectors, as can be noted from equation (52) with $S(n, t) =$ constant $(=\gamma_\sigma/3)$. (No cross-correlation exists for the chain at $t = 0$ affinely deformed from the isotropic, equilibrium state.) Thus, for this chain, the transient dynamics during the creep process and the non-instantaneous part of $J_r(t)$ (equation (59)) are exclusively attributed to this growth of cross-correlation. (For the four-bead chain, the non-instantaneous part is contributed from this growth as well as from the evolution of the anisotropy of respective bond vectors.)

In relation to this result, it is informative to remember the creep behaviour of the two-bead chain having a single bond vector. For this chain, no cross-correlation exists and no transient (delayed) conformational change occurs during the creep process. Correspondingly, its $J_r(t)$ has a constant value $(=1/\nu k_B T)$ over the entire range of t.

Now, we turn our attention to the creep recovery behaviour shown in the right halves of the panels in figures 9 and 10. At the onset of recovery ($t = 0$), the four-bead and three-bead chains exhibit abrupt jumps of the σ_p, S, and S_R values from respective values in the steadily flowing state. As shown in equations (54)–(56), this jump is the same in magnitude as that at $t = 0$ in the creep process but occurs in the opposite direction. Since $[\sigma_p(0)]_{\text{creep}} = \sigma_0/(N-1)$ for all p and $[S(n, 0)]_{\text{creep}} = \sigma_0/3G(0) = \gamma_\sigma/3$ for all n, the magnitude of the abrupt jump at the onset of recovery is the same for all eigenmodes and/or all bond vectors. This result indicates that the steadily flowing chain is affinely deformed on sudden removal of the stress by the magnitude γ_σ in the direction opposite to the flow, as explained in more detail in appendix C.

For the four-bead chain after this affine deformation, $\sigma_p(t)$, $S(n, t)$, and $S_R(t)$ gradually decay to zero; see figure 9. This behaviour reflects the interplay among all eigenmodes and/or all bond vectors occurring under the constant stress (zero-stress) requirement, similarly to the situation during the creep process.

For the three-bead chain, $S(n, t)$ immediately decays to zero at the onset of the recovery because of the equivalence of all (two) bond vectors; see figure 10(b). However, the transient changes of $\sigma_p(t)$ during the recovery process (figure 10(a)) demonstrate that the chain gradually change its conformation through the interplay of the eigenmodes under the zero-stress requirement. The gradual decay of $S_R(t)$ (figure 10(b)) is exclusively attributed to a decay of the cross-correlation associated with this interplay. This situation is similar to that seen for the creep process.

3.3.4. Similarity/difference between discrete and continuous Rouse chains. The fundamental feature of the discrete Rouse chains with $N = 3$ and 4, the transient conformational changes during the creep/recovery processes governed by the interplay among all eigenmodes and/or among all bond vectors, remains the same for the chains with any N value. Indeed, the interplay (due to the constant stress requirement) governs the creep/recovery behaviour of the continuous Rouse chain with $N \to \infty$, as demonstrated earlier.

Here, we focus on the other feature of the discrete chains, the affine deformation on sudden imposition/removal of the stress observed through the normalized orientation function, $S^\circ(n, t) = \{\nu(N-1)k_B T/\sigma_0\}S(n, t)$ $(=S(n, t)/\gamma_\sigma)$. For the continuous chain, $S^\circ(n, t)$ during the creep and recovery processes is shown in figures 2(b) and 3(b). As seen in figure 2(b), $S^\circ(n, t)$ at short t during creep ($t = 0.01\tau_R$) is independent of n and has a value of $1/3$ except for the segments near the chain ends ($n \cong 0, N$). Indeed, from equations (21) and (30), we can confirm $[S^\circ(n, 0)]_{\text{creep}} = 1/3$ at $t = 0$ over the entire range of $0 < n < N$. This result indicates that the continuous chain is affinely deformed from the isotropic, equilibrium

state by the magnitude γ_σ ($=\sigma_0/\nu N k_B T$ in the continuous limit for $N \to \infty$) at the onset of creep.

Furthermore, equations (30) and (34) give a relationship between the eigenmode anisotropies during the creep and recovery processes of the continuous chain, $[A_p(t)]_{\text{recovery}} = [A_p(\infty)]_{\text{creep}} - [A_p(t)]_{\text{creep}}$. Through equation (21), this relationship is rewritten as $[S(n,t)]_{\text{recovery}} = [S(n,\infty)]_{\text{creep}} - [S(n,t)]_{\text{creep}}$. That is, equation (55) is valid also for the continuous chain. Since $[S(n,0)]_{\text{creep}} = \gamma_\sigma [S^\circ(n,0)]_{\text{creep}} = \gamma_\sigma/3$, this chain has an n-independent difference, $[S(n,0)]_{\text{recovery}} - [S(n,\infty)]_{\text{creep}} = -\gamma_\sigma/3$. This result, identical to that found for the discrete chains, indicates that the continuous chain is affinely deformed from the steadily flowing state at the onset of creep recovery.

Thus, the discrete and continuous chains commonly exhibit the affine deformation by the magnitude of γ_σ on sudden imposition/removal of the stress. However, we also note a quantitative difference: since the strain characterizing this deformation, $\gamma_\sigma = \sigma_0/G(0) = \sigma_0/\nu(N-1)k_B T/\sigma_0$, decreases with increasing N, the discrete chain exhibits discontinuous jumps of finite magnitude in its σ_p, S, and S_R on sudden imposition/removal of the stress (see figures 9 and 10) while only infinitesimal jumps are observed for the continuous chain with $N \to \infty$ (as can be noted from equations (29), (30), and (34)). This difference naturally results in a difference in the instantaneous value of the recoverable compliance of these chains; $J_r(0) > 0$ for the discrete chains (equations (48) and (59)) while $J_r(0) = 0$ for the continuous chain (equation (27)).

This feature of $J_r(0)$ has an important consequence for experiments: when we attempt to describe viscoelastic data for real polymer chains at short t with the Rouse model, the chains should be subdivided into the actual Rouse segments with the size being intrinsic to each polymer. This size can be determined experimentally with the aid of the modified stress optical rule [15]. Extensive experiments by Inoue and co-workers suggest that the Rouse segment size is close to the Kuhn segment size [15–17].

3.4. Difference between retardation and relaxation properties

For the chains obeying the Rouse dynamics as well as another type of molecular dynamics such as reptation, the viscoelastic properties characterizing the creep and relaxation processes are equivalent in the sense that the chain conformation evolving through the given dynamics is averaged in these properties (and these properties are mutually related through equation (1)). However, the chain has different conformations during the creep and relaxation processes because of the constant stress requirement in the former process, as fully discussed in the early part of this article. A corresponding difference is noted for the viscoelastic properties characterizing these processes. This section discusses this difference for some simple examples.

3.4.1. Recoverable compliance for Rouse and Doi–Edwards models. The Doi–Edwards (DE) model based on the tube concept has been frequently utilized for entangled polymers [4–6]. Since this model considers just the reptative diffusion along the chain backbone and does not incorporate other important mechanisms (such as the contour length fluctuation [18–21] and constraint release [20–23]), its prediction does not quantitatively agree with experiments. Nevertheless, the DE model captures fundamental physics in the entanglement dynamics and is well established as the starting model for entangled polymers. We here compare the creep behaviour for the DE and the Rouse models.

The relaxation modulus of the DE model is given by [4–6]

$$G(t) = G_N \sum_{p=1}^{\infty} \frac{8}{(2p-1)^2\pi^2} \exp\left(-\frac{(2p-1)^2 t}{\tau_{\text{rep}}}\right) \tag{61}$$

where G_N and τ_{rep} are the plateau modulus and pure reptation time, respectively. Pearson and co-workers [24] analytically calculated the compliance $J(t)$ corresponding to this $G(t)$ by conducting Laplace inversion of the convolution relationship (equation (1)). Their result can be summarized as

$$J_{\text{r}}(t) = \frac{1}{G_N} + \frac{2}{G_N} \sum_{p=1}^{\infty} \frac{1}{\theta_p^2} \left\{1 - \exp\left(-\frac{t}{\lambda_p}\right)\right\} \qquad \text{with } \lambda_p = \frac{\pi^2 \tau_{\text{rep}}}{4\theta_p^2} \quad \text{for DE model} \tag{62}$$

where θ_p is the numerical coefficient determined from equation (28). That is, the coefficients θ_p determining the retardation times λ_p and retardation intensities $2/G_N\theta_p^2$ of the DE model are identical to those for the Rouse model. Thus, the relative distributions of the retardation modes are identical for the two models; see equations (27) and (62).

The DE model has a non-zero $J_{\text{r}}(0)$ value ($=1/G_N$) while the continuous Rouse model has $J_{\text{r}}(0) = 0$ (see equation (27)). However, this difference is not essential because the discrete Rouse model has $J_{\text{r}}(0) > 0$. From this point of view, the $J_{\text{r}}(t)$ of the two models are surprisingly similar to each other, despite the fact that the relaxation modulus of the Rouse model, $G(t) = \nu k_{\text{B}}T \sum_{p=1}^{\infty} \exp(-tp^2/\tau_{\text{R}})$ in the continuous limit, is significantly different from $G(t)$ for the DE model.

The Rouse dynamics allows the viscoelastic relaxation to occur at any part of the chain, while the reptation dynamics allows the relaxation to occur only from the chain ends. This difference is clearly reflected in $G(t)$ for the DE and Rouse models but not so clearly in the non-instantaneous part of $J_{\text{r}}(t)$. This fact demonstrates the difference between the creep and relaxation properties.

3.4.2. Combination of Rouse and reptation mechanisms [14]. The difference between the creep and relaxation properties can be more clearly tested for a chain relaxing through multiple mechanisms. As the simplest test, we here examine $G(t)$ and $J_{\text{r}}(t)$ for a chain relaxing through the reptation and Rouse mechanisms.

This chain is assumed to have the relaxation modulus given by

$$G(t) = 2B \sum_{p=1}^{\infty} \exp\left(-\frac{p^2 t}{\tau_{\text{R}}}\right) + G_N \sum_{p=1}^{\infty} \frac{8}{(2p-1)^2\pi^2} \exp\left(-\frac{(2p-1)^2 t}{\tau_{\text{rep}}}\right). \tag{63}$$

Here, $2B$ is a parameter representing the relaxation intensity for the Rouse process. Considering the importance of the contour length fluctuation (CLF) for real chains composed of a finite number (Z) of entanglement segments of the molecular weight M_e (not the Rouse segments), we assume the Rouse process to occur along the whole backbone of the chain (not only within the entanglement segment). For this case, the ratio of the longest viscoelastic Rouse relaxation time $\tau_{\text{R}}(\propto Z^2)$ to the pure reptation time τ_{rep} is given by [4–6]

$$r_\tau = \frac{\tau_{\text{R}}}{\tau_{\text{rep}}} = \frac{1}{6Z}. \tag{64}$$

In a refined molecular model for entangled chains such as the Milner–McLeish (MM) model [21], the reptation time and relaxation mode distribution change with the CLF contribution. In addition, the MM model treats separately two series of the Rouse relaxation modes within the entanglement segment and along the whole backbone of the chain. However, these refinements are not considered in the simple calculation presented here, because the

purpose of this calculation is to examine the difference between the creep and relaxation properties. Qualitative features of the calculated results would not be affected by these refinements. (If the CLF mode is neglected in the MM model, $G(t)$ for this model becomes very similar to that given by equation (63).)

The intensity parameter for the pure Rouse mechanism is given by $2B = \nu k_B T$, and the plateau modulus is (experimentally) expressed as $G_N = Z\nu k_B T$ [3–5]. The combination of the Rouse and reptation mechanisms would not significantly change the values of $2B$. Thus, for simplicity and definiteness, we utilize the neat Rouse parameter $2B = \nu k_B T = G_N/Z$ in the following calculation.

For $G(t)$ given by equation (63), the recoverable compliance $J_r(t)$ can be analytically obtained through equation (1) with the Laplace inversion method. The result is summarized as [14]

$$J_r(t) = \varphi_0 - \sum_{p=1}^{\infty} \varphi_p \exp\left(-\frac{t}{\Lambda'_p}\right) \qquad \text{with } \Lambda'_p = \frac{\pi^2 \tau_{rep}}{\alpha_p^2} \quad (p\text{th retardation time}) \tag{65}$$

with

$$\varphi_0 = \frac{2(3G_N + 8Br_\tau^2)}{5(G_N + 4Br_\tau)^2} \tag{66}$$

and

$$\varphi_p = \frac{2}{G_N \tan^2(\alpha_p/2) + B\alpha_p^2 r_\tau - G_N\left\{\frac{\tan(\alpha_p/2)}{(\alpha_p/2)} - 1\right\}\{1 - \alpha_p\sqrt{r_\tau}\cot(\alpha_p\sqrt{r_\tau})\}}. \tag{67}$$

The coefficients α_p appearing in equations (65) and (67) are determined from

$$\frac{\tan(\alpha_p/2)}{(\alpha_p/2)} = 1 + \frac{B}{G_N}\{\alpha_p\sqrt{r_\tau}\cot(\alpha_p\sqrt{r_\tau}) - 1\} \tag{68}$$

with r_τ being the relaxation time ratio specified by equation (64).

In the limit of $B \to 0$, equation (68) reduces to equation (28) with $\theta_p = \alpha_p/2$ and $J_r(t)$ coincides with the reptation compliance (equation (62)). In the other limit of $G_N \to 0$ while keeping $B > 0$, equation (68) reduces to equation (28) with $\theta_p = \alpha_p\sqrt{r_\tau}$ and $J_r(t)$ coincides with the Rouse compliance (equation (27)).

In figure 11, a normalized recoverable compliance $J_r(t)G_N$ calculated from equations (65)–(67) for $Z = 10$, 20, and 50 is plotted against a normalized time t/λ_1 (unfilled symbols). For comparison, $J_r(t)G_N$ for the pure reptation dynamics (equation (62)) is shown with the solid curve. The dotted curves indicate $J_r(t)G_N$ (equation (27)) obtained for the Rouse chain having Z and τ_R identical to those utilized in equation (63). For the chain obeying equation (63), these dotted curves show the intrinsic Rouse behaviour that should be observed in the absence of the reptation contribution.

As can be noted in figure 11, the normalized compliance $J_r(t)G_N$ for $Z = 10$–50 (unfilled symbols) exhibits a crossover from the intrinsic Rouse behaviour (dotted curves) to the pure reptation behaviour (solid curve) with increasing t because the Rouse mechanism (having $G(0) = \infty$) dominates the creep behaviour at short t but this mechanism is overwhelmed by the slower reptation mechanism at long t. More importantly, a characteristic time for this approach to the reptation-dominant steady state deviates from the intrinsic, longest Rouse retardation time λ_R (at which the dotted curves level off).

In order to elucidate the origin of this deviation, it is useful to remember how the stresses $\sigma^{[1]}$ and $\sigma^{[2]}$ sustained by short and long Rouse chains in the blends evolve with time during the creep process (figure 6(a)): the short chain is mobile compared to the long chain and thus

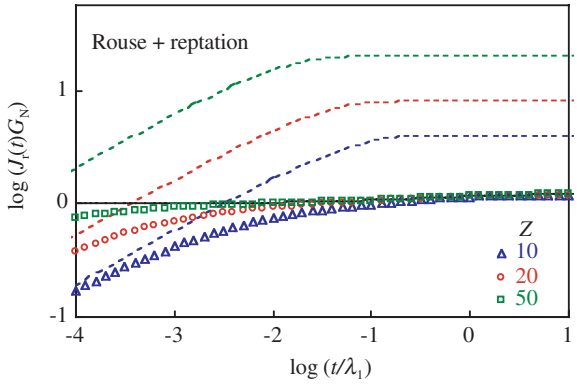

Figure 11. Plots of normalized recoverable compliance $G_N J_r(t)$ of the chain relaxing through Rouse and reptation mechanisms against normalized time t/λ_1 (unfilled symbols). The solid curve indicates $G_N J_r(t)$ for the pure reptation dynamics, and the dotted curves show the intrinsic Rouse behaviour of the chain.

forced to compensate the slow growth of $\sigma^{[2]}$ of the latter under the constant stress requirement. For this reason, $\sigma^{[1]}$ and $\sigma^{[2]}$ change in a synchronized way, and the intrinsic longest retardation time of the short chain is not resolved in the creep behaviour of the blend.

Equation (63) indicates that the stresses σ_R and σ_{rep} due to the Rouse and reptation mechanisms are additive. Thus, the Rouse mechanism being faster than the reptation mechanism plays a role similar to that of the short chain in the blend, and its σ_R is forced to compensate the slow growth of σ_{rep}. For this reason, the approach to the reptation-dominated steady state does not occur at the intrinsic λ_R, as observed in figure 11.

This situation can be even more clearly observed for a retardation spectrum $L(\lambda)$ defined by

$$J_r(t) = \int_{-\infty}^{\infty} L(\lambda)\left\{1 - \exp\left(-\frac{t}{\lambda}\right)\right\} \mathrm{d} \ln \lambda. \tag{69}$$

For $J_r(t)$ given by equation (65) as well as for $J_r(t)$ for pure Rouse and reptation mechanisms (equations (27) and (62)), the spectra are analytically expressed as sums of delta functions, $L(\lambda) = \sum_{p=1}^{\infty} I_p \delta(\ln \lambda - \ln \lambda_p)$. The plot of this $L(\lambda)$ against $\log \lambda$ looks like a crowded set of spikes, and characteristic features of the spectra are not so easily observed in this plot. For easy observation, we integrated the retardation intensities I_p in a given logarithmic interval of λ, $\Delta \log \lambda = 0.2$, to evaluate smoothed (smeared) spectra. These spectra correspond to those usually evaluated from experimental data [3].

In figure 12, the normalized spectra $L(\lambda)G_N$ thus obtained for $Z = 10$–50 are double-logarithmically plotted against a normalized retardation time λ/τ_{rep}. The unfilled circles represent $L(\lambda)$ for the combined Rouse–reptation mechanism (equation (63)), and filled squares and triangles denote $L_R(\lambda)$ and $L_{rep}(\lambda)$ for the pure Rouse and reptation mechanisms, respectively. The solid and dotted arrows denote the longest retardation times λ_R and λ_{rep} of the intrinsic Rouse and reptation mechanisms, respectively. The spectrum L (circles) clearly exhibits the crossover from the Rouse spectrum (squares) to the reptation spectrum (triangles) with increasing λ. However, no peak of L is observed at $\lambda \cong \lambda_R$, confirming the effect of the interplay of the Rouse and reptation mechanisms discussed above.

Furthermore, we also note that L exhibits a broad peak at $\lambda_{peak} = 10^{-4\pm0.5}\tau_{rep}$ and $10^{-5.5\pm0.5}\tau_{rep}$ for $Z = 20$ and 50, respectively; see the middle and bottom panels of figure 12. *Neither* the Rouse *nor* the reptation mechanism (the constituent mechanisms in the chain

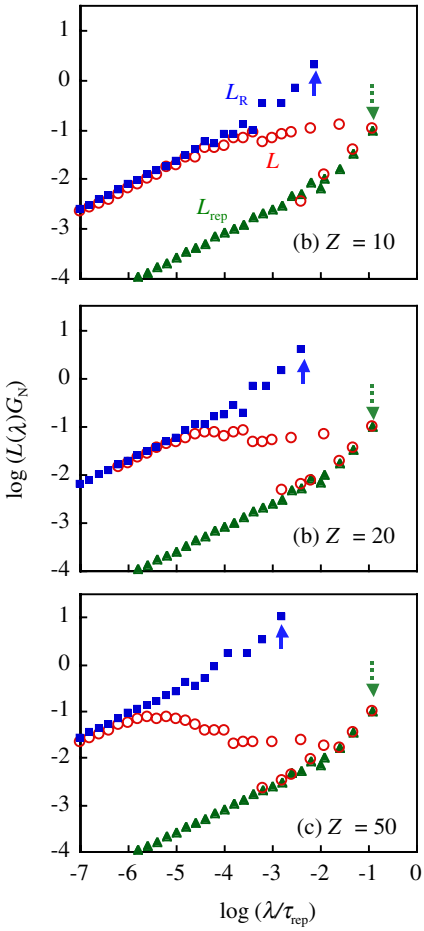

Figure 12. Normalized retardation spectra $L(\lambda)G_N$ corresponding to the recoverable compliance shown in figure 11.

dynamics) gives a motional mode of specific meaning at these λ_{peak}, and the peak of L results from the interplay of these mechanisms under the constant stress requirement. We may give a molecular interpretation to this peak on the basis of the knowledge about the constituent mechanisms: the Rouse relaxation time for the entanglement segment is given by $\tau_e = \tau_R/Z^2 = \tau_{rep}/6Z^3$. The above λ_{peak} values are reasonably close to the τ_e values ($=10^{-4.68}\tau_{rep}$ and $10^{-5.88}\tau_{rep}$ for $Z = 20$ and 50) and the peak of L can be qualitatively related to equilibration of the Rouse motion within respective entanglement segments (and a crossover to the reptative motion utilizing these segments as the motional unit).

For the chain relaxing through multiple mechanisms, the above result demonstrates that the peak of the retardation spectrum L is hard to interpret on the molecular basis *if the details of these mechanisms are not known*. Similarly, for materials obeying stress additivity, a peak of L is often observed experimentally but its molecular interpretation is not so easily established unless the interplay of the constituent mechanisms is specified. In contrast, a peak of the relaxation spectrum H of such materials is not affected by this interplay and can be interpreted more directly. This is an important difference between the retardation and relaxation properties.

Since the stress of polymer chains in the liquid state is directly related to their orientational anisotropy *except at very short timescales* [5, 6, 15–17], the polymeric materials obey stress additivity by nature. No simple strain additivity is found for these materials. In this sense, a detailed viscoelastic investigation of molecular dynamics in polymers is to be made for relaxation properties rather than for retardation properties, although these properties are equivalent on the phenomenological basis. This fact may provide us with a clue for resolving recent problems related to the validity of the stress additivity or strain additivity in the viscoelastic analysis of the polymer dynamics in the Rouse-to-rubbery zone [25–27] as well as in the vicinity of the glassy zone [25, 28, 29].

4. Concluding remarks

The Rouse model is one of the most important models in the field of polymer dynamics, but its conformational changes during the creep/recovery processes had not been analysed previously. For completeness of the analysis, we have analytically calculated the orientational anisotropy for the monodisperse Rouse chains and their blends. The calculation reveals that each Rouse eigenmode during these processes has a distribution in the retardation times and each retardation mode of the recoverable compliance is contributed from all eigenmodes because of the interplay among the eigenmodes of different orders (and for different chains in the blends) under the *constant stress* condition. This feature is quite different from that under rate-controlled flow where each eigenmode behaves independently. Furthermore, the calculation indicates that the Rouse chains exhibit affine deformation on sudden imposition/removal of the stress and the magnitude of this deformation, reflected in the instantaneous value of the recoverable compliance, is inversely proportional to the number of bond vectors per chain. These features can be tested from rheo-optical creep/recovery experiments for the real non-entangled chains having appropriate labels, for example, from dichroism experiments for chains having partial deuterium labels. Unfortunately, such a rheo-optical creep/recovery experiment has not been conducted so far. The experiment is now being attempted in order to test the above Rouse features under the constant stress condition.

On the basis of the above results, a difference between the creep and relaxation properties is also discussed for chains obeying multiple relaxation mechanisms (Rouse and reptation mechanisms). For polymers intrinsically obeying stress additivity (except at very short t), it is suggested that a detailed viscoelastic investigation of molecular dynamics should be made for relaxation properties rather than for retardation properties, although these properties are equivalent on a phenomenological basis.

Appendix A. Solution of equation (24)

For the Laplace transformation of the strain, $\Gamma(s) = \int_0^\infty \mathrm{d}t\, \gamma(t) \exp(-st)$, equation (24) is rewritten as

$$\frac{\sigma_0}{s} = \nu k_\mathrm{B} T \sum_{p=1}^{\infty} \frac{s\Gamma(s)}{s + p^2/\tau_\mathrm{R}}. \tag{A.1}$$

A relationship deduced from the initial condition for creep ($\gamma(0) = 0$), $\int_0^\infty \mathrm{d}t\, \dot{\gamma}(t) \exp(-st) = s\Gamma(s)$, has been utilized in the derivation of equation (A.1).

With the aid of a mathematical formula, $\sum_{p=1}^{\infty}(x^2 + p^2)^{-1} = (\pi/2x)\coth(\pi x) - x^{-2}/2$, equation (A.1) is rewritten as a simple expression for $\Gamma(s)$ in terms of the transformation variable s,

$$\Gamma(s) = \frac{2\sigma_0}{\nu k_B T} \frac{1}{s\{\pi\sqrt{s\tau_R}\coth(\pi\sqrt{s\tau_R}) - 1\}}. \tag{A.2}$$

As noted from the asymptotic behaviour, $[s\Gamma(s)]_{s\to 0} = \infty$ and $[s^2\Gamma(s)]_{s\to 0} = 6\sigma_0/\pi^2\tau_R\nu k_B T$, this $\Gamma(s)$ has a second-order pole at $s = 0$. Thus, $\Gamma(s)$ is divided into the second-order pole part $\{6\sigma_0/\pi^2\tau_R\nu k_B T\}s^{-2}$ and the remaining first-order pole part $\Gamma_R(s)$ as

$$\Gamma(s) = \left(\frac{6\sigma_0}{\pi^2\nu k_B T\tau_R}\right)\frac{1}{s^2} + \Gamma_R(s) \tag{A.3}$$

with

$$\Gamma_R(s) = \left(\frac{2\sigma_0}{\nu k_B T}\right)\frac{3 + \pi^2 s\tau_R - 3\pi\sqrt{s\tau_R}\coth(\pi\sqrt{s\tau_R})}{\pi^2 s^2\tau_R\{\pi\sqrt{s\tau_R}\coth(\pi\sqrt{s\tau_R}) - 1\}}. \tag{A.4}$$

$\Gamma_R(s)$ has first-order poles at $s = 0$ (with a residue $[s\Gamma(s)]_{s\to 0} = 2/5$) and at $s = s_p = -\theta_p^2/\pi^2\tau_R$ (with a residue $[(s - s_p)\Gamma(s)]_{s\to s_p} = -4/\theta_p^2$), where θ_p are numerical coefficients determined from

$$\tan\theta_p = \theta_p \qquad (p\pi < \theta_p < (p + 1/2)\pi \quad \text{and} \quad \theta_p \to (p + 1/2)\pi \quad \text{for } p \to \infty). \tag{A.5}$$

These coefficients satisfy summation rules, $\sum_{q=1}^{\infty}\theta_q^{-2} = 1/10$ and $\sum_{q=1}^{\infty}\{p^2 - (\theta_q/\pi)^2\}^{-1} = -3/2p^2$. Thus, the Laplace inversion of equation (A.3) gives

$$\gamma(t) = \frac{\sigma_0}{\nu k_B T}\left[\frac{6t}{\pi^2\tau_R} + \sum_{p=1}^{\infty}\frac{4}{\theta_p^2}\left\{1 - \exp\left(-\frac{t}{\lambda_p}\right)\right\}\right] \qquad \text{with } \lambda_p = \frac{\pi^2\tau_R}{\theta_p^2}. \tag{A.6}$$

Appendix B. Solution of equation (32)

For the Laplace transformation of the shear rate, $\Gamma'(s) = \int_0^{\infty} \mathrm{d}t\, \dot{\gamma}(t)\exp(-st)$, equation (32) is rewritten as

$$0 = \sum_{p=1}^{\infty}\frac{6\sigma_0}{p^2\pi^2}\frac{1}{s + p^2/\tau_R} + \nu k_B T\sum_{p=1}^{\infty}\frac{\Gamma'(s)}{s + p^2/\tau_R}. \tag{B.1}$$

With the aid of a mathematical formula, $\sum_{p=1}^{\infty}\{x^2 + p^2\}^{-1} = (\pi/2x)\coth(\pi x) - x^{-2}/2$, equation (B.1) is rearranged as

$$\Gamma'(s) = -\left(\frac{2\sigma_0}{\nu k_B T}\right)\frac{3 + \pi^2 s\tau_R - 3\pi\sqrt{s\tau_R}\coth(\pi\sqrt{s\tau_R})}{\pi^2 s\tau_R\{\pi\sqrt{s\tau_R}\coth(\pi\sqrt{s\tau_R}) - 1\}}. \tag{B.2}$$

Analysis of poles of this Γ' (similar to that in appendix A) enables the Laplace inversion of equation (B.2) to give

$$\dot{\gamma}(t) = -\frac{4\sigma_0}{\nu k_B T\pi^2\tau_R}\sum_{p=1}^{\infty}\exp\left(-\frac{t}{\lambda_p}\right) \qquad \text{with } \lambda_p = \frac{\pi^2\tau_R}{\theta_p^2} \tag{B.3}$$

with the coefficients θ_p being determined from equation (A.5).

Appendix C. Affine deformation and effective strain for the bond vector

For the Rouse chain during the creep/recovery processes in the linear viscoelastic limit, no correlation exists between the z component and x and y components of its bond vector $\mathbf{u}(n, t)$

at any time t. For this case, the bond vector can be expressed in terms of a reference vector $\mathbf{u}^*(n)$ as

$$\mathbf{u}(n,t) = \mathbf{D}(\gamma_e(n)) \cdot \mathbf{u}^*(n) \qquad \text{with } \mathbf{D}(\gamma_e(n)) = \begin{bmatrix} 1 & \gamma_e(n) & 0 \\ 0 & 1 & 0 \\ 0 & 0 & 1 \end{bmatrix}. \tag{C.1}$$

$\mathbf{D}(\gamma_e(n))$ is a shear displacement tensor corresponding to an effective shear strain $\gamma_e(n)$ defined for $\mathbf{u}(n,t)$; $\gamma_e(n) \ll 1$ and $\langle\{u^*_\alpha(n)\}^2\rangle/a^2 = 1/3 + \mathrm{O}(\gamma_e^2)$ ($\alpha = x, y, z$) in the linear viscoelastic limit. From equation (C.1), the orientation function of the nth bond vector, $S(n,t) = a^{-2}\langle u_x(n,t)u_y(n,t)\rangle$, is related to the function defined for the reference vector, $S^*(n) = a^{-2}\langle u^*_x(n)u^*_y(n)\rangle$, as

$$S(n,t) = \frac{1}{a^2}\langle(\mathbf{D}\cdot\mathbf{u}^*)_x(\mathbf{D}\cdot\mathbf{u}^*)_y\rangle = S^*(n) + \frac{\gamma_e(n)}{3}. \tag{C.2}$$

Here, we have neglected terms of the order of γ_e^2.

The affine shear deformation of the chain is defined as a deformation associated with n-independent effective strain ($\gamma_e(n) = \gamma_e$). If $\mathbf{u}^*(n)$ coincides with the isotropically distributed nth bond vector $\mathbf{u}^{\mathrm{eq}}(n)$ at equilibrium, $S^*(n) = 0$ and the affine deformation results in n-independent $S(n,t)$ ($=\gamma_e/3$) associated with no cross-correlation ($\langle u_x(n,t)u_y(m,t)\rangle = 0$ for $n \neq m$). The n-independence of the $S(n,t)$ value ($=\sigma_0/3G(0)$) and the lack of cross-correlation are found for the four-bead and three-bead chains as well as for the continuous chain with $N \to \infty$ at the onset of creep (at $t = 0$). Thus, at the onset of creep, the chain is affinely deformed from the isotropic, equilibrium state by the strain $\gamma_\sigma = \sigma_0/G(0)$. On this deformation (without the cross-correlation), the orientation function S_R of the end-to-end vector defined by equation (52) is written as $S_R(0) = S(n,0) = \sigma_0/3G(0) = \gamma_\sigma/3$. This $S_R(0)$ value is found for the chains at the onset of creep (see equations (53) and (58)), confirming the affine deformation explained above.

If the reference vectors, $\mathbf{u}^*(n)$ with $1 \leqslant n \leqslant N-1$, are non-uniformly oriented, the orientation function $S^*(n)$ defined for these vectors is non-zero and dependent on n. For this case, we note from equation (C.2) that the affine deformation of these reference vectors gives an n-independent difference, $S(n,t) - S^*(n) = \gamma_e/3$. For the four-bead and three-bead chains as well as for the continuous chain, this n-independent difference is found at $t = 0$ for the creep recovery, $[S(n,0)]_{\mathrm{recovery}} - [S(n,\infty)]_{\mathrm{creep}} = -\sigma_0/3G(0) = -\gamma_\sigma/3$. Thus, at the onset of recovery, these chains are affinely deformed from the non-uniformly (non-affinely) oriented flowing state by the strain of $-\gamma_\sigma$.

On this affine deformation, the orientation function $S_R(0)$ of the end-to-end vector $\mathbf{R}(0)$ is related to the function defined for the reference vectors,

$$S^*_R = \frac{1}{N-1}\left\{\sum_{n=1}^{N-1} S^*(n) + \sum_{n,m(\neq n)=1}^{N-1} S^*_c(n,m)\right\} \qquad \text{with } S^*_c(n,m) = a^{-2}\langle u^*_x(n)u^*_y(m)\rangle_{n\neq m},$$

as

$$\begin{aligned} S_R(0) &= \frac{1}{N-1}\left[\sum_{n=1}^{N-1} S(n,0) + \frac{1}{a^2}\sum_{n,m(\neq n)=1}^{N-1}\langle\{u^*_x(n) + \gamma_e u^*_y(n)\}u^*_y(m)\rangle\right] \\ &= \frac{1}{N-1}\left[\sum_{n=1}^{N-1}\left\{S^*(n) + \frac{\gamma_e}{3}\right\} + \sum_{n,m(\neq n)=1}^{N-1}\left\{S^*_c(n,m) + \frac{\gamma_e}{a^2}\langle u^*_y(n)u^*_y(m)\rangle\right\}\right] \\ &= S^*_R + \frac{\gamma_e}{3} + \frac{1}{N-1}\frac{\gamma_e}{a^2}\sum_{n,m(\neq n)=1}^{N-1}\langle u^*_y(n)u^*_y(m)\rangle. \end{aligned} \tag{C.3}$$

The last term in equation (C.3) is of the order of γ_e^2 (because $\langle u_y^*(n)u_y^*(m)\rangle_{n\neq m} \sim \mathrm{O}(\gamma_e)$) and is overwhelmed by the $\gamma_e/3$ term. Thus, equation (C.3) gives an n-independent difference $S_R(0)-S_R^*$ that coincides with $S(n,t)-S^*(n) = \gamma_e/3$. For the four-bead and three-bead chains as well as for the continuous chain, this n-independence of the difference is found at the onset of the creep recovery, $[S_R(0)]_{\text{recovery}}-[S_R(\infty)]_{\text{creep}} = [S(n,0)]_{\text{recovery}}-[S(n,\infty)]_{\text{creep}} = -\gamma_\sigma/3$, confirming the affine deformation from the steadily flowing state.

References

[1] Rouse P E 1953 *J. Chem. Phys.* **21** 1272
[2] Graessley W W 1974 *Adv. Polym. Sci.* **16** 3
[3] Ferry J D 1980 *Viscoelastic Properties of Polymers* 3rd edn (New York: Wiley) p 183
[4] Pearson D S 1987 *Rubber Chem. Technol.* **60** 439
[5] Doi M and Edwards S F 1986 *The Theory of Polymer Dynamics* (Oxford: Clarendon) p 91
[6] Watanabe H 1999 *Prog. Polym. Sci.* **24** 1253
[7] Berry G C 1987 *J. Polym. Sci.* B **25** 2203
[8] Lodge A S and Wu Y J 1971 *Rheol. Acta* **10** 539
[9] Lodge A S 1964 *Elastic Liquids* (New York: Academic) p 123
[10] Watanabe H and Inoue T 2004 *Rheol. Acta* **43** 634
[11] Watanabe H and Inoue T 2004 *Macromolecules* **37** 8167
[12] Magenau H and Murphy G M 1955 *The Mathematics of Physics and Chemistry* (New York: Van Nostrand-Reinhold) chapter 8
[13] Watanabe H and Inoue T 2004 *Korea–Australia Rheol. J.* **16** 91
[14] Watanabe H and Inoue T 2004 *Nihon Reoroji Gakakishi (J. Soc. Rheol. Japan)* **32** 113
[15] Inoue T, Okamoto H and Osaki K 1991 *Macromolecules* **24** 5670
[16] Inoue T and Osaki K 1996 *Macromolecules* **29** 1595
[17] Inoue T, Matsui H and Osaki K 1997 *Rheol. Acta* **36** 239
[18] Doi M 1981 *J. Polym. Sci. Polym. Lett. Edn* **19** 265
[19] Doi M 1983 *J. Polym. Sci. Polym. Phys. Edn* **21** 667
[20] Graessley W W 1982 *Adv. Polym. Sci.* **47** 68
[21] Milner S T and McLeish T C B 1998 *Phys. Rev. Lett.* **81** 725
[22] Klein J 1978 *Macromolecules* **11** 852
[23] Daoud M and de Gennes P G 1979 *J. Polym. Sci. Polym. Phys. Edn* **17** 1971
[24] Pearson D S, Mueller S J, Fetters L J and Hadjichristidis N 1983 *J. Polym. Sci. Polym. Phys.* **21** 2287
[25] Inoue T and Osaki K 1999 *Macromolecules* **32** 4725
[26] Roland C M, Archer L A, Mott P H and Sanchez-Reyes J 2004 *J. Rheol.* **48** 395
[27] Roland C M, Ngai K L and Plazek D J 2004 *Macromolecules* **37** 7051
[28] Roland C M and Mott P H 1998 *Macromolecules* **31** 7095
[29] Roland C M and Mott P H 1999 *Macromolecules* **32** 4728